




Article

Concept Design of the Underwater Manned Seabed Walking Robot

Asghar Khan ¹, Wang Liquan ^{1,*}, Wang Gang ², Muhammad Imran ¹,
Hafiz Muhammad Waqas ¹ and Asad A. Zaidi ³

¹ College of Mechanical and Electrical Engineering, Harbin Engineering University, Harbin 150001, China; asghar81@hrbeu.edu.cn (A.K.); mimran@hrbeu.edu.cn (M.I.); hafizwaqas@hrbeu.edu.cn (H.M.W.)

² College of Shipbuilding Engineering, Harbin Engineering University, Harbin 150001, China; wanggang@hrbeu.edu.cn

³ Department of Engineering Sciences, PN Engineering College, National University of Sciences and Technology, Karachi 75350, Pakistan; asadali@pnec.nust.edu.pk

* Correspondence: wangliquan@hrbeu.edu.cn; Tel.: +86-1393-600-0513

Received: 22 August 2019; Accepted: 11 October 2019; Published: 15 October 2019



Abstract: In this paper, a novel concept designed of a multi-legged underwater manned seabed walking robot is presented. The robot will be used in both shallow water current (1–2 m/sec) and deep water up to 500 m. It is powered by an external electric power source through tether cable. It walks on the seabed with six legs, which makes it distinct from conventional screw-propelled underwater robots. It can walk calmly without making the water turbid. Two anterior arms act as manipulators. All leg joints and manipulators are controlled by Brushless Direct Current Motors. Motivation for this concept comes from soldier crab that walk mostly forward and has an egg-shaped body. It is operated by a pilot sitting in a pressurized cabin, and promptly control operations of the robot and manipulator. Preliminary design of the pressurized cabin, using an empirical formula, “ASME PVHO-1 2007” standard, and validation was carried out through ANSYS Workbench. Hydrodynamic forces acting on the robot body and legs are utilized to withstand the water current and external forces to adjust legs and body posture for stability. Buoyancy rules are employed to control its rising and diving motion. All key technologies employed in the development of the robot and their approaching methods are explained. It will provide a safe operation space for humans in underwater operations.

Keywords: legged robots; spherical hull; metachronal gait; buoyancy control; acrylic viewport

1. Introduction

The planet is very vast and rich in many valuable resources. Human effort for exploiting such resources has been increased in the last few decades. There is yet a vast expanse of uncharted and unexplored territories on land and beneath the sea. The ocean is a big gift from nature, and very rich in such resources. However, only about 5% of the ocean has been explored by humans [1–3]. Prior to progress of underwater technology, it was dangerous and difficult to explore and exploit these underwater resources [4]. Underwater exploration and work is very challenging, expensive, and time-consuming in the deep sea. Due to a complex and dynamic underwater environment, the deployed system must avoid obstacles and compensate for various external disturbances like sea currents and drag effects [5]. Demand for underwater research and exploration is rapidly increasing. Underwater robotics is recognized as an entity with high economic and significant values in this regard [3]. These robots can be used in military operations, underwater mine detection and deactivation, for recreational purposes, for collecting oceanography data, and for the inspection of dams, ports, and nuclear power plants [6]. These robots may be used in studying underwater biological and

geographical phenomenon [7–9]. Significant research in the field of underwater biomimetic robots based on animals like fish, crabs, and lobsters has been carried out for studying the mechanisms for generating locomotion and navigation [10].

Numerous underwater vehicles have been developed using various methods and configurations for seabed exploration. Most of these studies deal with screw-driven Remotely Operated Vehicle (ROV) and Autonomous Underwater Vehicle (AUV) [11,12]. However, these vehicles have some drawbacks such as a low degree of precision in the underwater survey, a seabed disturbance by the propeller, and a low endurance capability in high tidal current. These vehicles become less valuable and less effective in such circumstances [13]. To overcome such problems, a seabed walking robot with multiple legs is an optimized solution [14]. A seabed walking robot with multiple legs is amongst the new emerging technologies in underwater research and development. Maritime and Ocean Engineering Research Institute (MOERI) in Korean Institute of Science and Technology (KIOST) has performed research on an underwater robot called “Crabster.” It flies across the seabed like a crab and walks with six legs in high tide areas like a lobster [15]. Wang Gang et al. [16] studied design principles of the subsea propulsion pattern called crab bounding gait for a crab-like robot. The concept of a hybrid leg-paddle driven crab-like robot was developed for a shoal area. The robot walks using six legs and swims by two paddles. Tanaka et al. developed an amphibious six-legged underwater walking robot, focused mainly on watertight joints, reduction of weight, and transformation of the on-land robot to an underwater robot [17]. Samuel N. et al. worked on the design and control of six-legged swimming and walking robot TURTLE for on-land, underwater, and above water applications [18]. Design and development of a six-legged underwater seabed walking robot CR200 for inspection and operation in high tidal and low visibility areas was carried out by KIOST [19–21]. Superiore Sant’Anna School Italy, worked on a six-legged Crab Robot SILVER-2 that walk on the seabed to collect plastic waste. It can adapt to the uneven seabed, bounce back without damage, and avoid dangers [22]. An underwater hexapod robot AQUA was developed that uses paddles for propulsion and control of its orientation. Its amphibious legs act as flippers during swimming on the surface and legs during walking on the seabed [23]. iRobot’s Ariel imitating crab is a six-legged robot capable of walking both on land and underwater in the turbulent surf zone [24].

Recently, thousands of underwater robots are used worldwide for underwater applications. Mostly, these robots are screw-propelled or legged robots with remote or autonomous control. In this article, we use a novel and different concept of legged robot that will perform underwater operations very efficiently and accurately. Some underwater applications such as pipeline inspection, marine life observation, underwater repair, and environmental disaster assessment involve stationary observation. It is a very complex and energy-consuming task for swimming and for thruster-driven underwater robots because they must actively control their thrusters and buoyancy in order to maintain pose and stability. For station keeping operations, legged robots are more attractive than swimming and thruster-driven robots. Hence, for stationary observation applications involving considerable distance movement and station keeping, the Underwater Seabed Walking Robot (UMSWR), which is capable of walking on the seabed, is a very attractive solution. More importantly, thruster-driven underwater vehicles and robots must be deployed and recovered from some certain depth of water to be able to maneuver. It is not possible for conventional underwater robots to be deployed from the sea side or operated in shallow water. UMSWR can be deployed and recovered in both deep water and shallow water. All ROVs, AUVs, and a multi-legged seabed walking robot are controlled and operated from outside platforms that make their design, control, and operations very complex and tidy. The feature that makes UMSWR distinct from other legged robots is the use of the pressure hull that accommodate the operator. It is operated by a single operator sitting in the pilot cabin that operates and controls its operations very promptly and on time. A pressurized cabin provides a safe space for the operator in deep-sea operation. It also provides a proper working condition for critical instruments that need protection against hydrostatic pressure and water exposure. The operator can see many parameters

on the control panel screen and take the necessary action when needed. It enhances the operation execution and control of the robot and, hence, the efficiency of the robot.

Most of the seabed legged walking and crawling robots are autonomously or remotely operated. This makes the control of such robots quite complicated. It needs more apparatus and sometimes involves more people to remotely operate the robot. As in the case of CR200, four people are required to operate and control the robot and its operations. The pilot controls its walking and posture while the co-pilot controls its manipulator, camera, and light via two separate computer systems. Navigator plans its motion and keeps tracking its path and position. The sonar engineer monitors the scanning sonar and other sensors [25]. This also needs an intensive coordination among all four operators. Similarly, other legged robots that are remotely operated, cannot accomplish their tasks efficiently, and a considerable delay may occur. The motivation for UMSWR partly comes from the DEEPSEA CHALLENGER submersible that is operated and controlled by a single pilot. UMSWR is operated and controlled by a single operator, which operates and controls the robot and its manipulator instantly. The main controls of the robot are shared between a joystick control and a graphic user interface (GUI), incorporating a touch screen display on the control panel. This gives the onboard pilot ample control and dexterity while enhancing its efficiency and precision. UMSWR is designed for some specific operations in the target area on the seabed. For task performance, the robot needs some station-keeping modes and the operator will focus on the manipulator operation and control. During locomotion, no manipulator activity is performed and the operator will focus on the locomotion of the robot. UMSWR is predominantly forward walking, moving slowly with a speed of 0.5 m/sec within a limited range of 500 m radius from the source ship. It has the ability to turn left or right and the navigation is very simple to control. Therefore, a single operator can control its forward locomotion, vertical motion, manipulation, and navigation from the control panel. Remotely-operated robots rely on their appliances that may sometimes give inaccurate results in the dynamic and complex sea environment. However, in the case of UMSWR, the operator inside the robot can go and see the real scenario very closely and visually and take the decisions instantly. Controlled by the operator onboard, some of the appliances are excluded for UMSWR as compared to the unmanned robot. Reducing the appliances and number of operators makes it simpler. The inclusion of the pilot in the robot adds the novelty to an underwater seabed walking robot. Manned seabed walking robots will enhance underwater operations' capabilities and will stimulate advances in ocean science and underwater explorations in the future.

2. Concept of Underwater Manned Seabed Walking Robot (UMSWR)

A novel conceptual design of the Underwater Manned Seabed Walking Robot (UMSWR) is presented. In this study, working principles and design practices of Submersible, AUVs, ROVs, and legged walking robots are combined in one single robot. UMSWR is developed to substitute screw-propelled and remotely operated legged robots for enhanced seabed operations. The purpose of this study is to design a man-controlled robot that can walk and work on the seabed calmly and efficiently. The robot is envisioned for exploration, inspection, pick & place, and repair of underwater installed systems. Concept design at an early stage of product development has a significant influence on factors such as costs, performance, reliability, and safety. Similar products and technologies can be used for reference and for transforming customer requirements into product concept design through some key characteristics. Customer requirements are summarized in the design consideration [26,27]. Concept design of marine craft mainly includes the study of regulations, preparing specifications, the environmental effect, cost, economics, and basic structural and hydrodynamic studies [28].

The main design considerations for the UMSWR robot are: (1) Eco friendly: robot is powered from an external source in the form of electrical power through a tether cable, so it adds no pollution to the sea directly. Secondly, it has no propeller. The motion is quite calm compared to screw-propelled robots and it performs quiet operations. Since the robot has slow speed, it does not make the sea water turbid and surrounding visibility is not affected. (2) Comply with International Standards and

Design Practice: For the design of the Pilot cabin, ASME Standard “ASME PVHO-1-2007” and Chinese Classification Society (CCS) rules are used. For the body hull designing standard Naval Architecture principles, practices of submersible and submarine are used. (3) Simple and easy operation: The robot is operated by a single pilot controlling all of its operations. The pilot cabin provided with all essential life-supporting necessities so that the task can be performed without fatigue and in a relaxed mode. (4) Operate underwater up to 500 m depth on the seabed: The robot is designed to be deployed and work in sea state 4 and recovered in sea state 5, with a maximum payload of 50 kg. (5) Perform operations of inspection, repair, pick, and place through a manipulator, which is an integral part of the robot.

UMSWR will endure and work on the seabed in high tidal current (2 m/s) and up to 500 m deep. Structure, body shape, and walking mechanism of the robot resemble that of the soldier crab that walks mostly forward. The soldier crab is shown in Figure 1. The soldier crab is egg-shaped and its length to width ratio is 1.24. In other crabs, it is less than 1 [29]. Similarly, our goal is to design a forward walking mechanism with minor lateral movements. The legs of the robot will be designed to be strong enough to carry weight of the body and payload, and withstand the hydrodynamic forces/moments caused by water current in uneven and unstructured terrain.



Figure 1. Blue Soldier crab: (a) Soldier crab during the resting position and (b) soldier crab while walking.

All the legs have a multi-degree of freedom with flexible motion. It allows the body of the robot to adjust its height above the seabed to avoid obstacles, and adjust its position for a specified task within its reach and orientation, according to the hydrodynamic situations. It has six legs. All are 4-DoF, used for walking on the seabed. It has two arms. Both are 6-DoF used as the manipulator and also for walking on uneven surfaces for enhanced stability. All joints are controlled by Brushless Direct Current (BLDC) electric motors. It has sensors for the sea current speed and direction, contact sensors for each foot, and torque/force sensors for each joint.

UMSWR controls joint angles based on detected information, adjusts legs, and body pose to withstand external forces and maintain stability. A well-designed six-legged robot has an optimized mechanical structure and efficient motion planning algorithm. A study by various people is completed on structure and movement of legs for different degrees of freedom, drive, and transmission systems carried out to get a higher power-to-weight ratio and stronger perception abilities [30–32]. Its ability to walk and work underwater on the seabed will make it a useful working platform for a variety of underwater applications. 3-D model of the concept design modeled in Pro/ENGINEER software, as shown in Figure 2.

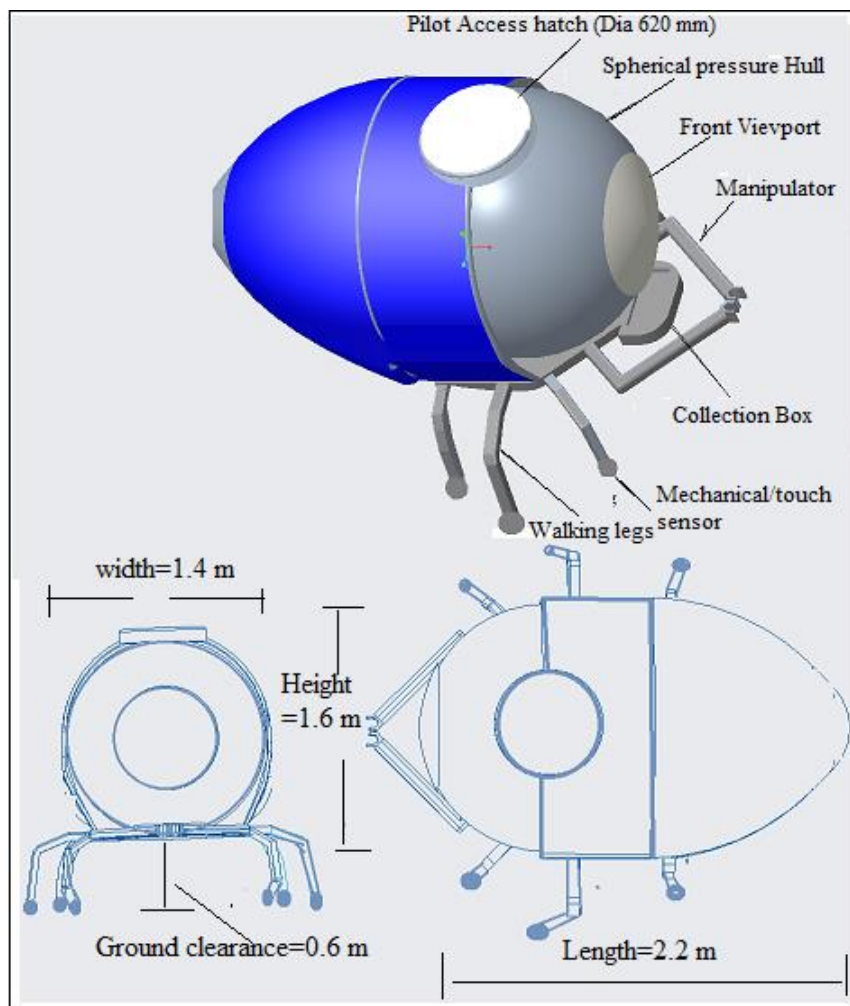


Figure 2. Conceptual design of UMSWR.

Working Concept of the UMSWR is shown in Figure 3. The robot is powered by some external source like a ship or any other floating platform through tether cable.



Figure 3. Operation concept of UMSWR.

The specifications of UMSWR are derived from a user requirements' analysis and concept design of the robot for the desired operation capabilities up to 500 m in depth. These specifications are listed in Table 1.

Table 1. Specifications of UMSWR.

Items	Specification Details
Maximum dimensions (LWH)	2.2 m × 1.4 m × 1.6 m
Maximum weight on surface	1000 Kg
Main ballast tank	1 m ³
Variable ballast tank	0.2 m ³
Maximum design depth	500 m
Payload capacity	50 kg
Maximum underwater speed	0.5 m/s
Operator/crew	Single operator/crew controlling all operations of the robot
Power	External power supply through a tether cable
Control	Controlled and operated by pilot-in-pilot cabin using a Control Joystick, touch screen, and manual override
Maximum operation endurance	Normal operation 8 hours + 72 hours emergency battery reserve for communication and instruments
Operating and recovery sea state	Working in sea state 4, recovery in sea state 5
Ground clearance	0.6 m
Life support	Oxygen and food/water for 72 hours
Pressure hull inner diameter	1.1 m
Pressure hull thickness	15 mm
Access hatch diameter	620 mm
Number of walking legs	6 walking legs (4-DoF), 2 manipulator arms (6-DoF)

3. Fundamental Technologies of the UMSWR

UMSWR is a combination of some fundamental technologies. Working principles and design practices of Submersible, AUVs, ROVs, and walking robots are combined in one single robot. We utilize existing and relevant technologies to develop UMSWR. Exploiting the Joint mechanism and walking technology of multi-legged on-land and underwater robots, waterproof and hydrodynamic technologies from AVU, ROV, and other underwater installed systems and Pressure hull technologies of submersible and submarine [21,33,34]. The utilization of these and other relevant technologies and their approaching methods to develop these technologies are discussed.

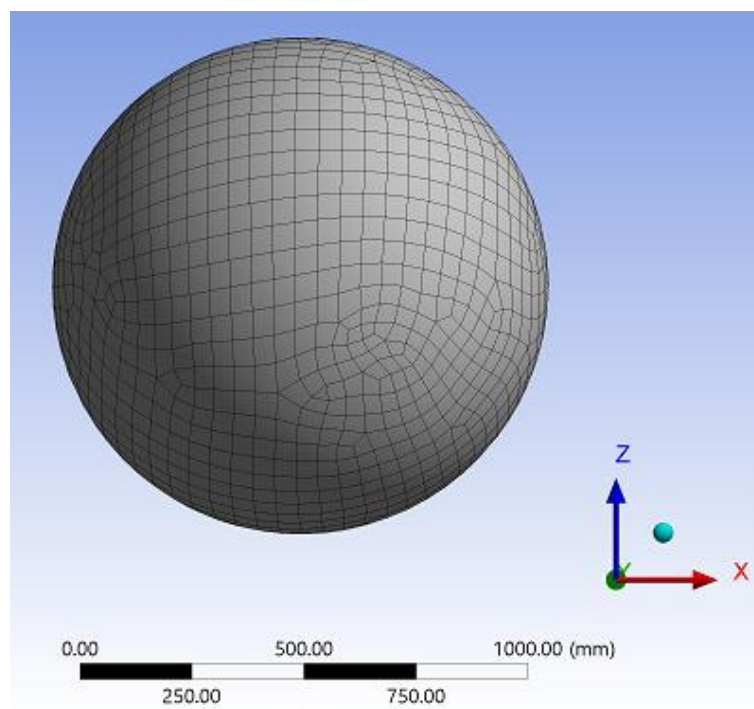
3.1. Design of the Pressurized Hull

The most critical component of the deep manned vehicle is the manned pressure hull that provides a safe living space for pilot and other crew members under the deep-sea pressure. Therefore, the pressure hull should be designed to have enough strength and should be as light as possible. Different classification societies use significantly different guidelines for the design of a spherical pressure hull and no unified approach exists for calculating thickness based on material failure and buckling instability [35]. In order to arrive at accurate and safer design, we employ different methods for finding out the thickness of the spherical pressure hull.

3.1.1. Finite Element Analysis

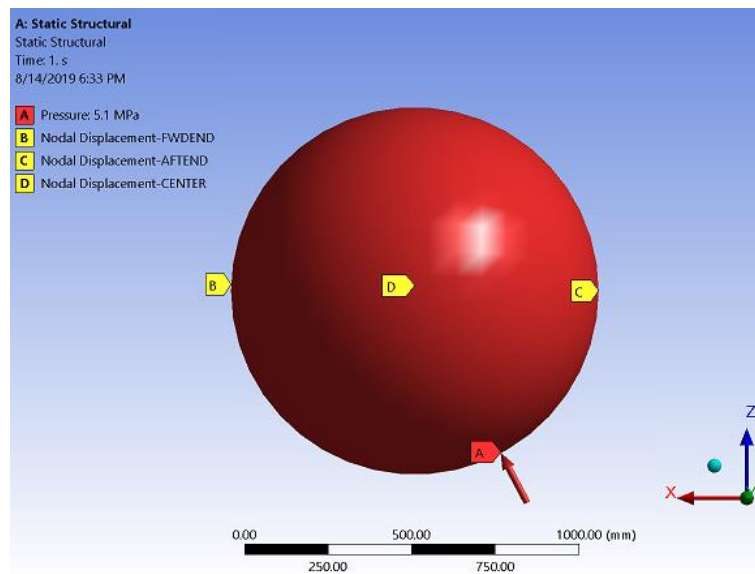
The most critical component of an underwater manned vehicle/submersible is the manned pressure hull that provides safe living space for the pilot and other crew members in the deep sea [36]. Various shapes such as cylindrical, spherical, and egg shapes have been used for constructing these pressure hulls. However, according to recent studies, spherical pressure hulls constructed with steels or other alloys have been demonstrated to have benefits over other shapes' pressure hulls. The benefits of the spherical hull are a very effective distribution of stress and displacement in the material and low buoyancy factor. Sphere is the shape with a minimum surface/volume ratio and the most suitable geometry to withstand external pressure with minimal weight [37]. The spherical hull has been used in submersibles like Alvin, Jiaolong, Nautile, RUS, and Shinkai6500 [32,38]. The diameter of the pressure hull is 1.1 m, which is almost consistent with the spherical hull of the Deep Sea Challenger with a single pilot of a 1.09 m diameter [39]. The pressure hull is designed to descend to 500 m, which corresponds to 5 MPa hydrostatic pressure. In order to determine the minimum thickness requirement under 5 MPa

hydrostatic pressure, a parametric study of the spherical pressure hull is carried out in the ANSYS Workbench. In the parametric study, a static structural analysis is performed and the thickness and Von-Mises stress are parameterized. Then the data is transferred to an eigenvalue buckling analysis for calculating the buckling load factor. In the Eigenvalue buckling analysis, the buckling factor is parameterized. Afterward, parametrization of the design variables and values for the thickness of the pressure hull are defined. The whole project is then updated and the required value of thickness of the spherical hull is calculated against Von-Mises stress and the buckling strength factor. The model of the hull is generated using primitive spherical features of the design modeler of ANSYS Workbench. The geometric model of the spherical hull is then meshed with shell elements of approximately 50 mm in size. Boundary conditions are applied to both the ends and the center of the pressure hull. According to Chinese classification society (CSS) rules, displacement at the aft and forward end should be fixed in the y and z directions and displacement near the center of the hull should be fixed in the xy or xz directions, as shown in Figure 4 [40]. The material of the pressure hull is Titanium Alloy, which can work underwater very well and has been proven in so many projects [41]. Two salient features of pure titanium metal are corrosion resistance and the strength-to-density ratio is the highest of any metallic element [42]. Lightweight and high-strength Titanium alloy (Ti-6Al-4V) has been used for most of the submersible and submarine hull [43]. Its properties are given in Table 2. The result of the parametric study for pressure hull thickness is shown in Figure 5. Von-mises stress and buckling strength factor are 160.57 MPa and 1.5, respectively. Results of the hull thickness versus the Von-mises stresses and the Buckling strength factor (λ) are shown in Figure 6. It can be noted from Figure 6a that the value of the Von-Mises stress rapidly decreases with the increase in the value of pressure hull thickness (t) from 0–4 mm. Beyond this point, a gradual decrease can be observed in the value of Von-mises stress. Similarly, the value of the buckling strength factor increases linearly with the increase in the value of pressure hull thickness (t) (Figure 6b). At a 1.5-factor of safety for buckling strength, the value of pressure hull thickness is 8 mm.



(a)

Figure 4. Cont.

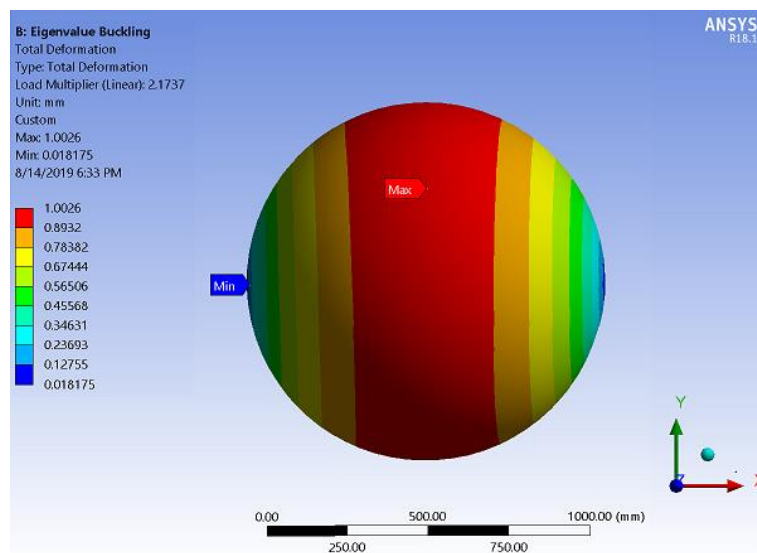


(b)

Figure 4. Spherical hull, (a) meshing, (b) boundary conditions, and loading.

Table 2. Properties of Titanium alloy (Ti-6Al-4V).

Young's Modulus E (MPa)	Yield Strength σ_y (MPa)	Tensile Strength σ_t (MPa)	Poisson Ratio μ	Density ρ (Kg/m ³)
115,000	830	869	0.3	4450



(a)

Figure 5. Cont.

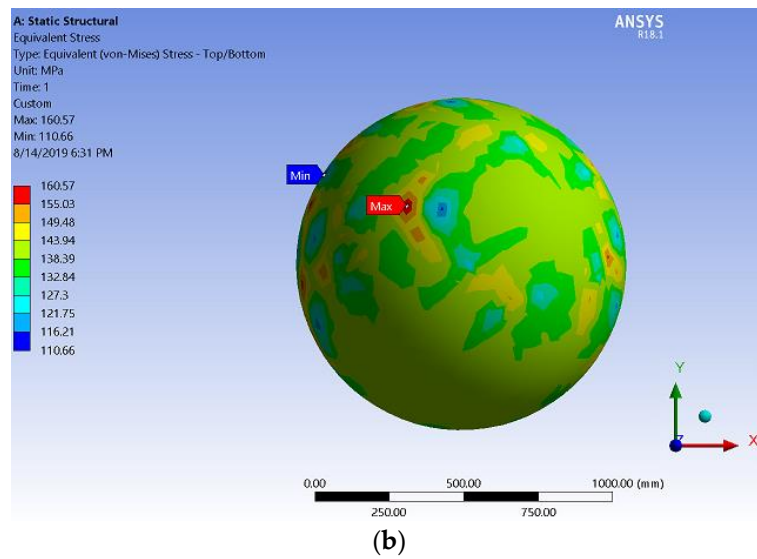
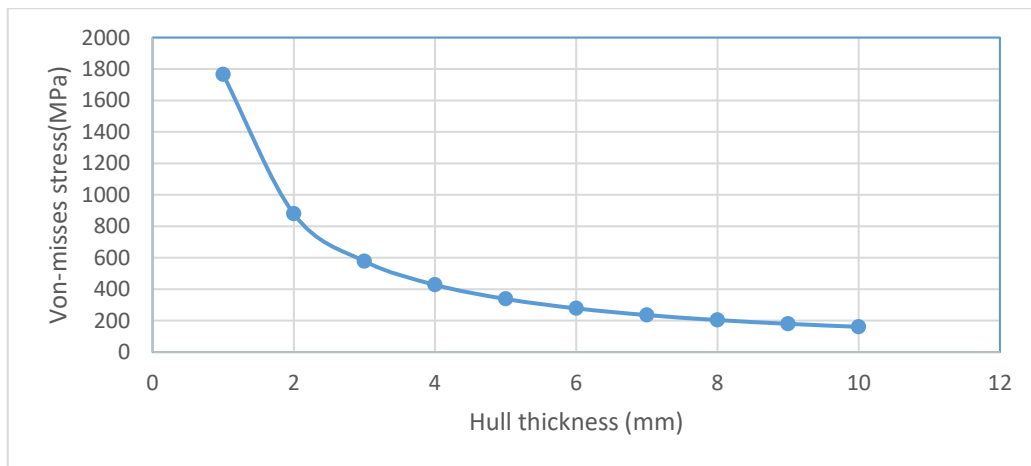
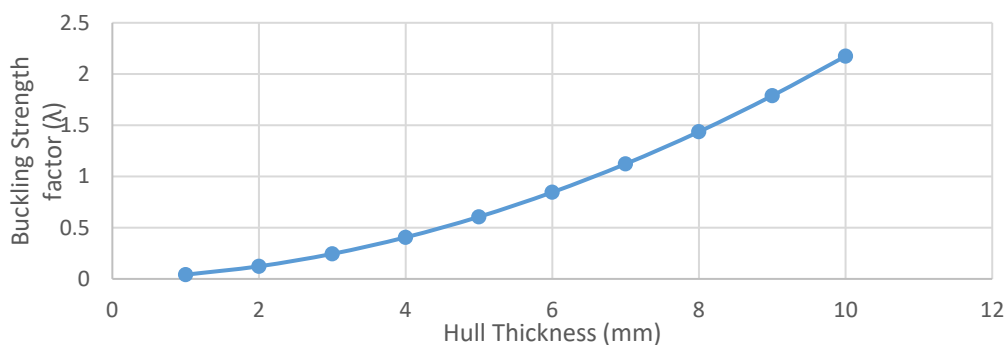


Figure 5. Spherical hull analysis, (a) Eigenvalue buckling, and (b) Von-misses stresses.



(a)



(b)

Figure 6. (a) hull thickness vs. Von-misses stress. (b) Hull thickness vs. Buckling Strength Factor (λ).

3.1.2. Analytical Calculations

Many theoretical and experimental studies have been carried out for calculating the load-carrying capacity of spherical shells under external pressure. Each classification society has its own way of calculating minimum thickness for a deep-sea manned spherical shell. To develop a consistent calculation method for predicting ultimate strength of the spherical pressure hull under external

pressure, many people have worked in this regard [38,44–48]. For a perfectly designed underwater spherical shell, there are two possible failure modes. These are: (1) maximum stresses in the shell reaching the yield condition and, consequently, yielding zone spread, which results in final plastic collapse. (2) Elastic or elastic–plastic buckling leads to collapse. The minimal external pressure of these two failure modes is defined as the ultimate strength of the sphere in Figure 7.

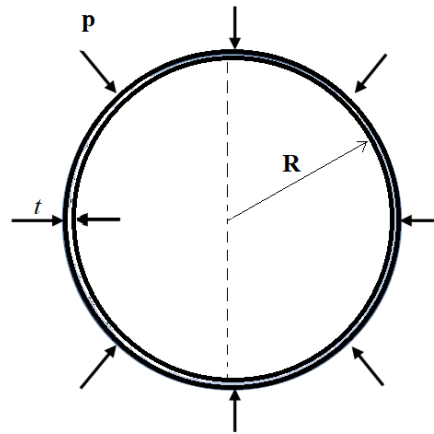


Figure 7. Perfect sphere subjected to external pressure underwater.

The hydrostatic pressure on the robot and, hence, the sphere is given by the formula below.

$$p = \rho gh \tag{1}$$

where “ ρ ” density of sea water (1025 kg/m³), “ g ” gravitational acceleration (9.8 m/s²), and “ h ” depth of water (500 m). Putting these values into Equation (1), we get pressure at the deepest point of 5.0 MPa. Keeping the factor of safety at 1.5, the test pressure or critical pressure is 7.5 MPa. For the yield condition, the value is calculated by using Formula (2).

$$\sigma = \frac{PR_m}{2t} \tag{2}$$

where “ σ ” is Stress in the sphere (N/m²), “ P ” is external pressure (N/m²), “ R_m ” is the main radius of the sphere (m), and “ t ” is the thickness of the sphere (mm). For spherical shells, the critical elastic buckling load under external pressure is given by Formula (3).

$$p_{cr} = \frac{2E}{\sqrt{3(1-\mu^2)}} \left(\frac{t}{R_m} \right)^2 \tag{3}$$

where “ E ” is the modulus of elasticity and “ μ ” is the Poisson ratio. Formulas (2) and (3) can be used to calculate the stresses in a perfect spherical shell under uniform external pressure. These two classical formulas are more theoretical and the latter were modified by Von Karman and Tsien [49]. They developed Formula (4), after many experimental works.

$$p_{cr} = 0.37E \left(\frac{t}{R_m} \right)^2 \tag{4}$$

The minimum required thickness for the spherical shell exclusive of corrosion allowance shall be determined by the following procedure as per the AME PVHO-1 2007 standard [50].

Calculate the value of C from Equations (5) and (6).

$$C_1 = \frac{0.75PT}{\sigma_y} \tag{5}$$

$$C_2 = \sqrt{\frac{1.79PT}{E}} \tag{6}$$

where PT represents the test pressure, and $C = \text{Larger of } C_1 \text{ and } C_2$, putting values in Equations (5) and (6), $C_1 = 0.0067$ and $C_2 = 0.01$. The larger value comes for $C_2 = 0.01$. The value of C calculated from Equations (5) and (6), while moving horizontally to an intersection with the solid curve on Figure 8.

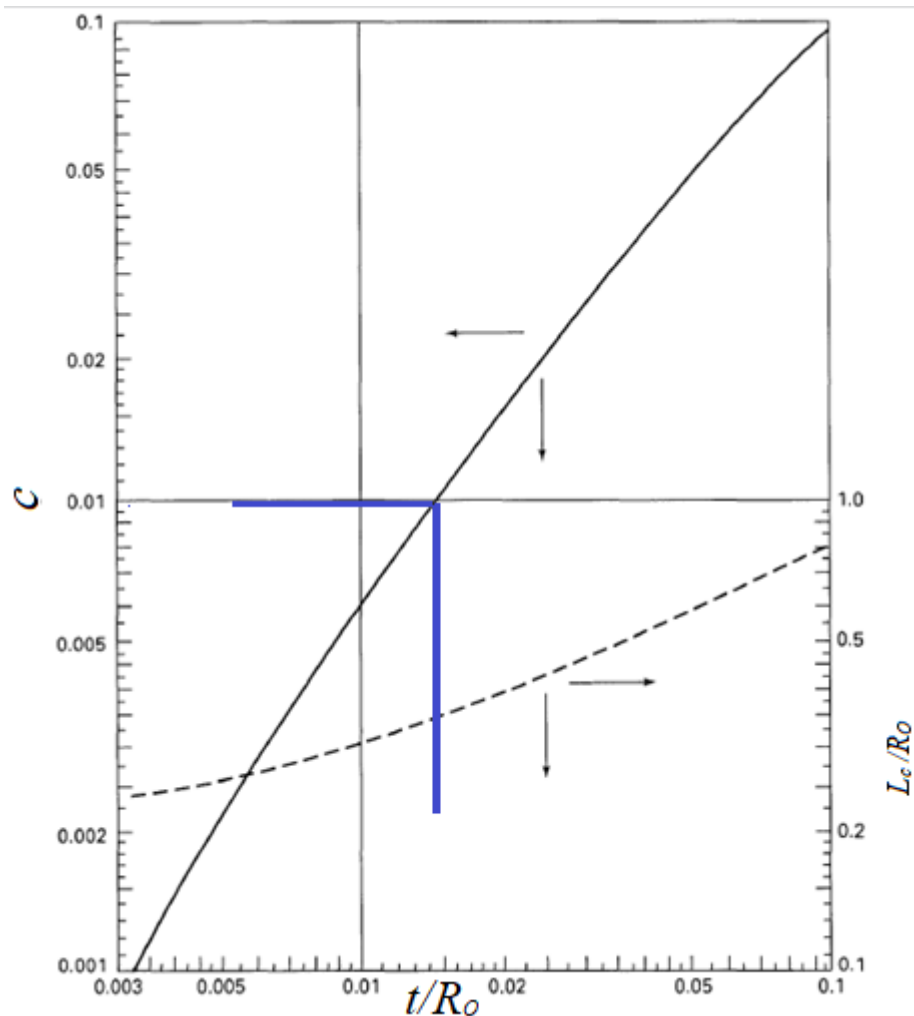


Figure 8. Values of $\frac{t}{R_0}$ and $\frac{L_c}{R_0}$ with the permission of The American Society of Mechanical Engineers, 2007.

From the intersection, moving vertically down and reading the value of the required minimum ratio of thickness to the outside radius ($\frac{t}{R_0}$). This value is 0.0145, approximately. This required minimum ratio applies to the spherical shell for the Titanium alloy (Ti-6Al-4V), the selected material for the spherical hull for its yield strength, elastic modulus, and test pressure (7.5 MPa). Determined the minimum required thickness t for the given radius. The value of t is approximately 8 mm. The values of the pressure hull thickness (t) obtained both from finite element analysis and analytical calculations are listed in Table 3. The minimum shell thickness, excluding corrosion allowance, shall not be less than 10 mm [50]. Calculated values of the spherical shell thickness using the empirical Formula (2) and (3) are 3 mm and 5.2 mm, respectively, giving a maximum value in buckling. The value of thickness evaluated by using Formulas (4), (5), and (6) are 7.5 mm and 8 mm, excluding corrosion allowance. Ultimately, from a concept design purpose, thickness is 12 mm including corrosion allowance.

Table 3. Results of the various methods applied for a thickness calculation.

Method Applied	Formula/Approach Applied	Calculated Thickness (mm)
Yield Stress	$\sigma = \frac{PR_m}{2t}$	3
Buckling Stress	$p_{cr} = \frac{2E}{\sqrt{3(1-\mu^2)}} \left(\frac{t}{R_m}\right)^2$	5.2
Von Karman and Tsien Experimental formula	$p_{cr} = 0.37E \left(\frac{t}{R_m}\right)^2$	7.5
ASME PVOH-1 2007	Standard procedure	8
ANSYS Workbench 18.1	Simulation	8

3.1.3. Design of the Viewport Window

Access hatch is provided on the top portion of the spherical pressure hull for entry and exit of the pilot. Two viewports with one in the access hatch and the other in the front section, help the pilot to drive the robot and make better observations of seabed and manipulator operation. For the design of acrylic viewports, the pilot utilizes empirical procedures of ASME PVHO-1 and a proven approach. The two viewports are spherical sectors, with opening angles of 90° in the front section and 60° in the top hatch. Acrylic windows with square edges are selected, as shown in Figure 9 and Equation (7).

$$\begin{aligned}
 D_i &= 2R_i \sin \frac{\alpha}{2} \\
 D_o &= 2t + D_i \\
 l &= t \sin \left(90 \text{deg} - \frac{\alpha}{2} \right)
 \end{aligned}
 \tag{7}$$

where D_i is the internal diameter, D_o is outside the diameter, t is the thickness, l is the length of the square edge, and α is the included angle of viewport. Acrylic is a thermoplastic with excellent environmental stability, low water absorption, good light transparency, and low density. Acrylic properties are shown in Table 4. Acrylic is used in underwater applications for the last few decades showing good results [33,37]. Windows are preliminarily designed for an external view that withstands the design pressure in a wide range of conditions of operations of the robot.

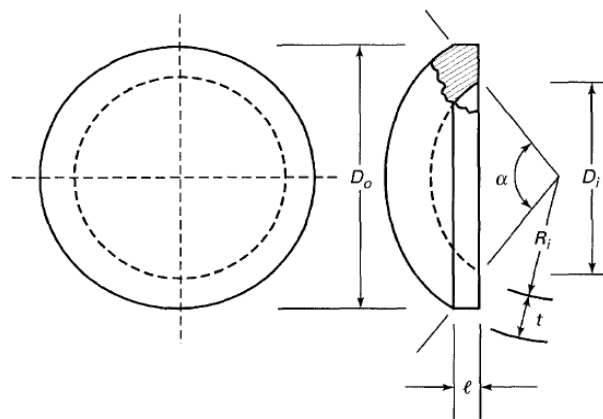


Figure 9. Viewport window of the acrylic with square edges [50].

Table 4. Properties of acrylic.

Light Transparency	Water Absorption (in 24 hours)	Density (Kg/m ³)
92%	0.25%	1190

Minimum acceptable thickness ratios shall comply with the requirements of Figure 9. Dimensions of the standard window in the design pressure range is based on window’s short-term critical pressure

(STCP) and the approved conversion factor (CF) for a given maximum average ambient temperature of 20 °C (24 °C inside and 16 °C outside).

$$STCP = CF \times P \tag{8}$$

where “CF” is the conversion factor and *P* is the design pressure. For a spherical sector window with square edges from ASME PHOV-1, CF = 6.5. Therefore, from Formula (8), STCP = 32 MPa. For STCP, the *t/D_i* value from the graph is 0.12. This implies *t* = 90 mm. The design life of spherical sector windows with the square edge, shown in Figure 9, and meeting the requirements of this standard will be 10 years from the date of fabrication. According to Reference [50], the hatch must have a nominal diameter of at least 610 mm for normal personnel entry and exit. We take 620 mm for a more convenient entry and exit. After the calculation, the hatch viewport included the angle and becomes approximately 60 degrees. On each side of the hatch, a handle is mounted for opening and closing it.

3.1.4. Total Mass of the Spherical Pressure Hull

The calculation of mass of the robot in marine application in the concept design phase is one of the key steps. The mass of the pressure hull is calculated below.

Volume of the sphere is given by Equation (9).

$$V = \frac{4}{3}\pi r^3 \tag{9}$$

$$V = \frac{4}{3}\pi[(r_1)^3 - (r_2)^3] \tag{10}$$

where *V* is the volume, *r₁* is the outer radius, and *r₂* is inner radius of the sphere. The volume of the sphere can be calculated by putting values in Equation (10).

$$V = \frac{4}{3} \times 3.14(0.562)^3 - \frac{4}{3} \times 3.14(0.550)^3$$

$$V = 0.744 - 0.697 = 0.047 \text{ m}^3$$

Mass of the hull is given by Equation (11).

$$m_T = \rho \times V \tag{11}$$

where *m_t* is the mass of the titanium spherical hull and *ρ_t* is the density of the titanium alloy from Table 2.

$$m_T = 210 \text{ Kg}$$

Since there are two holes of 60 degrees and 90 degrees, respectively, for the access hatch and the front viewport, which are subtracted from the above calculated value of the hull mass. The mass of the spherical pressure hull after subtracting the viewports’ portion given by Equation (12).

$$m_t = 210 \times \frac{210}{360} = 130 \text{ Kg} \tag{12}$$

Similarly, calculating the mass of the acrylic viewports with calculated thickness of 90 mm by adapting the same procedure. Mass of the total 150 degree acrylic viewport is calculated by the equation below.

$$m_{Acr} = \rho \times V \times \frac{150}{360} \tag{13}$$

$$m_{Acr} = 1190 \times 0.4 \times \frac{150}{360} = 200 \text{ Kg}$$

where m_{Acrr} is the mass of Acrylic viewports.

$$\text{Total mass of spherical pressure hull} = m = m_{Acrr} + m_t = 330 \text{ Kg}$$

The approximate mass of the pilot cabin is 330 kg. The UMSWR resemble the submersible. The weight of the pressure hull is almost 1/3 of the total weight of the submersible [51]. Therefore, the preliminary weight of the robot is approximately 1000 kg.

The pilot cabin will be equipped with systems to monitor and control the oxygen and carbon dioxide level, primary life support parameters such as potable water and food for normal and emergency situations, medical First Aid Box, and Lifejacket. System for monitoring humidity, temperature, and pressure of occupied space will also be installed. Two independent pressure gauges for depth registration will be installed. One of these will be functioning in an emergency situation, as a soon-rated depth of robot exceeds the depth alarm, which will give a warning. For two-way communication of the pilot with personnel at a support facility both on the surface and working underwater, a dual channel underwater telephone system (UWT) will be installed. Batteries for the emergency power supply, alarm indicating water leakage into the pilot cabin, battery pods, and other portions will be installed in a pilot cabin.

3.2. Joint Technology and Walking Mechanism

UMSWR has six legs for walking on the seabed and two arms for manipulating specific tasks. In some circumstances, the arms can also be used for walking. This combination gives the robot enhanced stability both while working and walking on the seabed. Underwater joint technology is the second to pilot cabin in UMSWR. Joint technologies used in multi-legged land and underwater robots considering the watertight corrosion and the effect of hydrodynamic and hydrostatic forces will be used [3,52,53]. UMSWR has a total of 36 joints and all these joints are controlled by Brushless Direct Current (BLDC) electric motors, with one for each joint. We select low-speed high torque BLDC Motors. For controlling and observing the angular position, absolute encoders will be installed at all joints of the legs. Legs are the main load carrying elements of the robot, so light weight, water resistance, and high strength material selection is needed for this purpose. All the legs and arms consist of links and joints, connected in series. All links and joints canisters are made of Aluminum (Al 6061) as it works very well in water. Aluminum is remarkable for its good strength (Young modulus 70 GPA), low density, and its ability to resist corrosion underwater. Electrical wirings and appliances making it waterproof is very critical and important. To make the motors and motor controllers against water secure, integrated watertight joint modules will be utilized. For both static and dynamic parts, the O-ring will be used for making it watertight.

In UMSWR, three joints for each leg are sufficient to walk but we use four joints instead. This increases the flexibility and avoids redundancy of legs to walk on uneven terrain of the seabed. Second, it allows the robot legs and body to adjust its posture against water current or any other disturbing force. Model leg and its link-joint system is shown in Figure 10. For joints and the walking mechanism, we imitate the soldier crab in its structure and configuration. All legs project normally to the curved sideline of the body that provide supporting points all around the body, as shown in Figure 11. The left forward, middle, and rear legs are numbered as 1, 2, and 3. Similarly, the right forward, middle, and rear legs are numbered as 4, 5, and 6, respectively. Arms are installed anteriorly, Leg 1 anterolateral, leg 2 laterally, and leg 3 posterolateral, with equal and wide spacing. This allows the legs more room for swinging backwards and forwards. The weight of legs is approximately 60% of the total weight of the robot [14]. Therefore, the estimated weight of each leg of UMSWR is 50 Kg. For a preliminary calculation, the range of rotation of each joint and length of each link is given in Table 5.

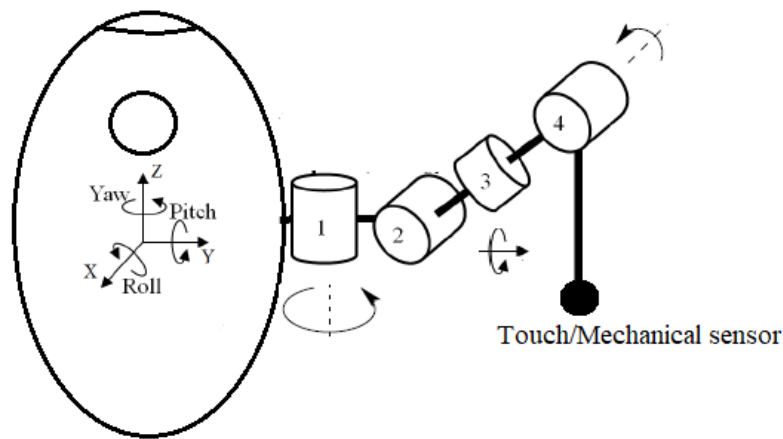


Figure 10. Concept design of the leg and joints.

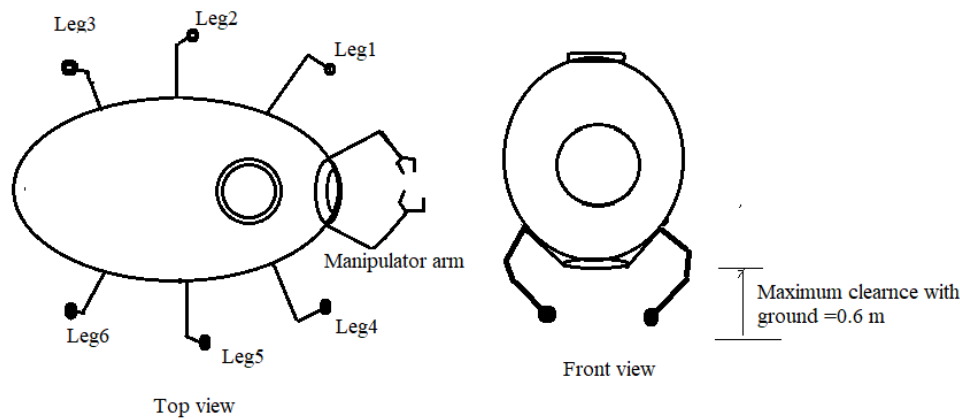


Figure 11. Robot legs' arrangement schematic.

Table 5. Specifications of UMSWR links and joints.

Joint/Link Number	1	2	3	4
Joint range rotation	$-50^{\circ} \sim +50^{\circ}$	$-90^{\circ} \sim +20^{\circ}$	$-180^{\circ} \sim +180^{\circ}$	$-90^{\circ} \sim +0^{\circ}$
Length of links (mm)	100	500	400	400
Maximum Speed of the Joint (rpm)	50	40	40	40

Joint ranges' and links' length of UMSWR are determined on the basis of soldier crab data. For joint 1, the rotation range about its origin is $-50^{\circ} \sim +50^{\circ}$. This defines the range of movement of joint 1, which allows anterior-posterior movements of the robot leg. This is the optimum rotation range for joint 1 that avoids a possible collision of the legs with each other during walking. Similarly, all other joints ranges are based on close similarity with joint ranges of the soldier crab by taking into consideration the allowable movements of the links. All links' lengths are adjusted such that the leg provides optimum ground clearance, a significant distance per step, and redundancy avoidance.

Leg configuration with (0, 0, 0, 0) in a fully extended pose has a total length of 1.4 m. The right hand rule is employed for an angle of the rotation direction. Joint 1 allows legs to swing forward and backward in order to promote a remote-causing forward movement of the robot. Joints 2 and 4 bend in the same plane and allow the leg to adjust the length and pose accordingly, which gives it more flexibility. Joint 3 is used to adjust the leg on an inclined plane that further enhances its flexibility for uneven terrain. It improves dynamic performance such as a posture maintenance at an uneven surface of the seabed and a posture adjustment in a shallow sea with high tidal current. During forward walking, gaits and phase of legs on both sides of the body are the same because contralateral legs share the load of the body equally. Maximum clearance of the robot body with the ground is 0.6 m.

The stepping patterns of UMSWR is such that legs show a metachronal wave of stepping. The legs step sequentially from 1 to 3. There is no overlap in the commencement of metachronal gait. Leg 1 is not placed a second time until all other legs have touched once. Each leg only lifts when the leg behind it is on the ground in the position to support robot weight. This creates a purely metachronal gait, 123, posteriorly directed, as shown in Figure 12. For example, between the start of leg 1 stepping twice at *a* and *b*, every other leg steps one time. This rhythm runs with equal duration to legs on both sides of the body. This provides increased stability and reduces the energy consumed. One complete step of the UMSWR takes approximately 1 s. The average speed of the robot on the seabed is 0.5 m/s.

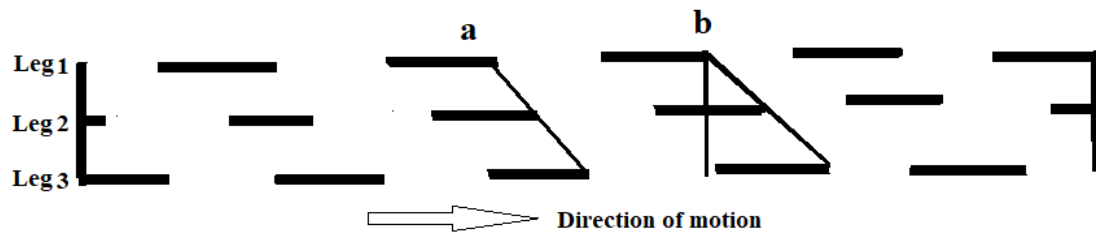


Figure 12. Metachronal gait of UMSWR.

Maximum required angular velocity and torque of each joint are calculated independently through simple static or dynamic force analysis. Based on these calculated values, the electric motors, reduction gears, and sensors are selected. Joint 1 is used for the forward motion and its angular velocity (ω) can be determined by Equation (14), as shown below.

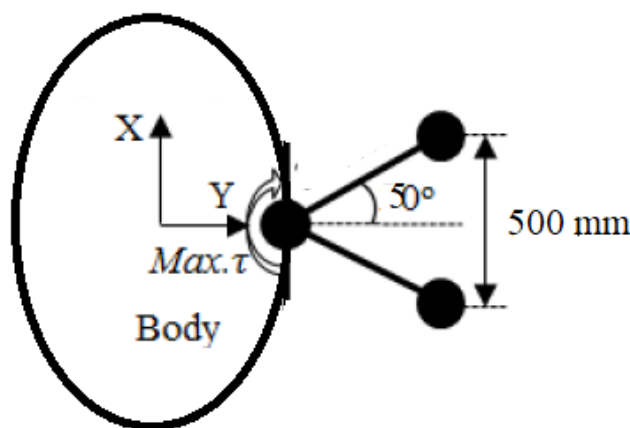
$$\omega = \text{joint speed} = \text{Number of revolutions} / \text{time} \tag{14}$$

In case of UMSWR, one complete step of the robot takes 1 second. Each leg of the robot on both sides takes the same time in stepping. Therefore, forward movement of joint 1 of each leg takes $\frac{1}{6}$ of a second. For joint 1 as shown in Figure 13, the speed can be calculated by putting values in Equation (14).

$$\omega_1 = \left(\frac{50 \text{ deg}}{360} \right) \div \frac{1}{6} \text{ second} = \frac{6 \times 50 \text{ deg}}{360 \text{ deg}} \frac{\text{revolution}}{\text{second}}$$

$$\text{Or } \omega = \frac{6 \times 50 \text{ deg}}{360 \text{ deg}} \times 60 = 50 \text{ rpm}$$

$$\omega_1 = \frac{6 \times 50 \text{ deg}}{360 \text{ deg}} \times 60 = 50 \text{ rpm} \tag{14a}$$



□

Figure 13. Configuration for deriving angular velocities.

Joint 2 and 4 are used only for posture transformation. Their motion is a standing motion in which it is assumed that the change time of joint 2 and 4 is one second. Therefore, the angular velocity of joint 2 and 4 is determined as 40 revolutions per minute. Lastly, angular velocity of joint 3 is also determined as 40 revolutions per minute.

The maximum torque required for each joint is calculated through simple static or dynamic force analysis. We consider an extreme posture in which the total weight of UMSWR is supported by five legs. For torque calculation, Equation (15) is used.

$$\tau = F \times D \tag{15}$$

where τ represents torque ($N \cdot m$), F is the force joint supports (N), and D is the moment arm (m).

Torque of joint 2 is calculated from the posture, as shown in Figure 14a. It is assumed that joints 1 and 3 are fixed and the shanks of feet are upright on the horizontal plane. The torque of joint 2 is calculated as 988 N·m. Similarly, torque for joint 4 is determined the same way as for joint 2. The value of torque for joint 4 is 988 N·m. The extreme loaded condition for joint 1 is shown in Figure 15a. In this condition, joint 2, 3, and 4 are fixed and all the loads of the leg are supported by joint 1. This occurs during the swing mode of the leg. Therefore, from Figure 15a, the torque for joint 1, according to Equation (15) is 343 N·m.

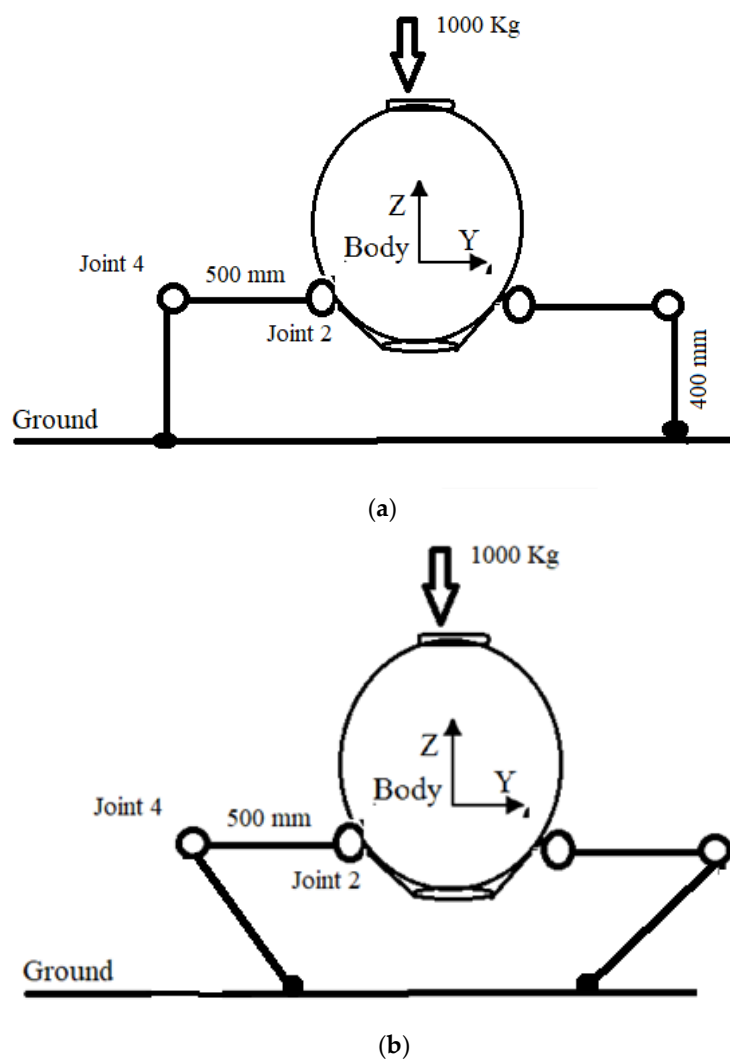


Figure 14. Extreme posture with the body supported by five legs, (a) payload joint 2, and (b) payload joint 4.

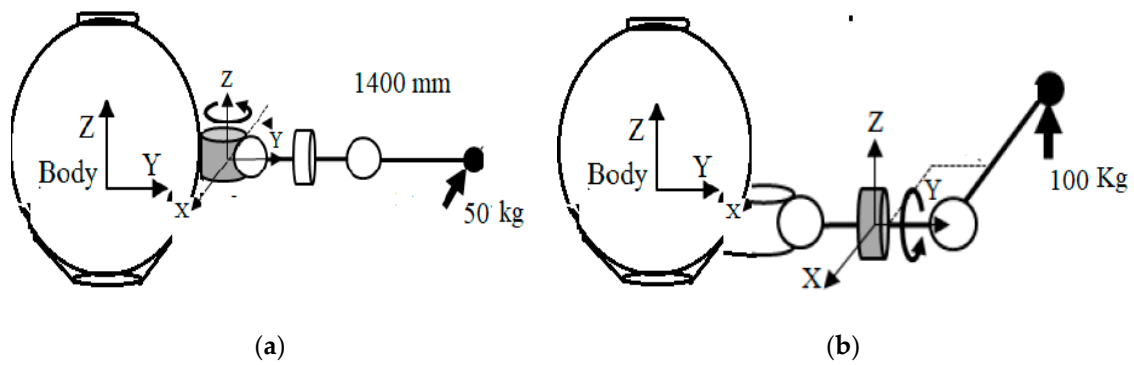


Figure 15. (a) Extreme load at joint 1 and (b) extreme load at joint 3.

Lastly, to derive the required torque of joint 3, it is assumed that the weight of 100 Kg is loaded at the end of the leg. The torque of joint 3 is calculated as 392 N·m.

$$\tau_a = \tau \times 1.15 \tag{16}$$

The maximum required torque for each joint is obtained by adding a safety factor of 1.15, as indicated by Equation (16) due to torque loss and inertial forces. The results with an added safety are given in Table 6.

Table 6. Maximum required torque.

Joint No	Required Torque (N·m)	Maximum Torque with Factor of Safety 1.15 (N·m)
1	343	400
2	988	1136
3	392	450
4	988	1136

For UMSWR, the speed of forward walking is controlled by joint 1. The average speed of the robot is determined below.

$$\begin{aligned} \text{Joint 1 speed} &= 50 \text{ rpm} \\ 50 \text{ rev} &= 1 \text{ min} \\ \text{time for 1 rev} &= 1/50 \text{ min} \\ \text{time for 1 rev} &= 60/50 \text{ sec} = 1.2 \text{ sec} \end{aligned}$$

Let the robot be in such a position that joint 1 is at a 0 degree position.

$$\text{Time taken by } 50^\circ \text{ rev} = 1.2 \times \frac{50}{360} = 0.16 \text{ sec} \tag{17}$$

$$\text{The time taken by one step} = \text{time taken by one step} \times 6 = 0.16 \times 6 = 1 \text{ sec} \tag{18}$$

Therefore, the robot covers 1 step/sec. One step of the robot in its average and optimum walking covers 0.5 m. Hence, the speed of the robot is approximately 0.5 m/sec. Evaluating angular velocities and torques in all joints, power consumption can be determined for each joint and, ultimately, for the whole robot. Power consumption in each joint is given by Equation (19).

$$P_{ij} = \tau_{ij}(t) \cdot \omega_{ij}(t) \tag{19}$$

where P represents power while $i = 1-6$ for leg and $j = 1-4$ for the joint. For UMSWR, the total power consumption is given by Equation (20).

$$P_{total} = \sum_{i=1}^6 \sum_{j=1}^4 P_{ij}(t) \tag{20}$$

The average power consumption can be evaluated by Equation (21).

$$P_{av} = \left(\frac{P_{tot}}{\left(\frac{T}{h}\right)} \right) \tag{21}$$

where T is the total time during which the robot is in motion and h is the step length. Specific energy consumption is given by Equation (22).

$$E_{sp} = \frac{P_{av}}{m_{tot} g v} \tag{22}$$

where E_{sp} is the specific energy consumption, m_{tot} is the total mass of the robot underwater, g is the gravitational acceleration, and v is the body velocity of the robot. The value of E_{sp} is used as an index of energy efficiency of the crab robot.

3.3. Modeling and Analysis of Hydrodynamic Forces

A hydrodynamic study and analysis is an important factor in the research of underwater robots and vehicles. Modeling and analysis of hydrodynamic forces on the robot body and legs is considered as third key technology in UMSWR because it is one of the main elements that affects its design. The efficiency and accuracy of the control algorithm and structure optimization of the robot mainly depend on hydrodynamic analysis. Many researchers have carried out research on hydrodynamics of underwater robots and vehicles [54–56]. Hydrodynamic forces can be analyzed experimentally as well as by numerical analysis tool (ANSYS, Star CCM+) and an empirical formula.

For control and optimized posture of legs with respect to hydrodynamic forces, it is necessary to model the hydrodynamic forces acting on the legs and robot body. Hydrodynamic forces and moments induced by relative water flow on legs and body are investigated. Lift force, forward drag force, and pitching moment are more important because they are related to stability, rollover, and slip of the robot. In hydrodynamics, the generalized hydrodynamic forces on a rigid body are linearly superimposed [57]. In order to exploit physical properties of models, equations of motion are represented in a vectorial setting. It is useful to exploit the physical system properties to reduce the number of coefficients needed for control [58]. The vectorial model is expressed in a body reference frame and an inertial reference frame, so appropriate kinematic transformations between these reference frames may be derived. The vectorial model is well-suited for computer implementation and control system design. The robot legs consist of joints and links and each link is subjected to various forces. It is supported by a reaction force and torque from the preceding link and is subjected to its own weight as well as the reaction forces and torques from the links that it supports. The overall dynamic equations of motions can be written in matrix form by Equation (23).

$$\tau = M_v(\dot{v}) + C_v(v)v + D_v(v)v + G_v(\eta) \tag{23}$$

$$\text{Where } \eta = [x, y, z, \theta, \phi, \psi]^T \tag{24}$$

$$v = [u, v, w, p, q, r]^T \tag{25}$$

where v and η are vectors of joint angles and position, respectively. M_v represent the inertia matrix including added mass, C_v is Coriolis, and the centrifugal term is caused by a rigid body and added

mass, D_v is hydrodynamic drag and lift force term, G_v is buoyancy and gravity term, and τ is the joint torque vector. We use the Newton-Euler formulation method to analyze the dynamics of the robot. In the Newton-Euler formulation, we treat each link of the robot one-by-one and write down the equations describing its linear and angular motion. Since each link is coupled to two other links, equations describing a link contain coupling forces and torques that appear in the equations of neighboring coupled links. We use forward-backward recursion to determine all of these coupling terms and arrive at a description of the robot leg and, consequently, the robot as a whole. It calculates the forces and moments acting on each link and, thus, joint torques. The free body diagram of forces and moments on link i is shown in Figure 16.

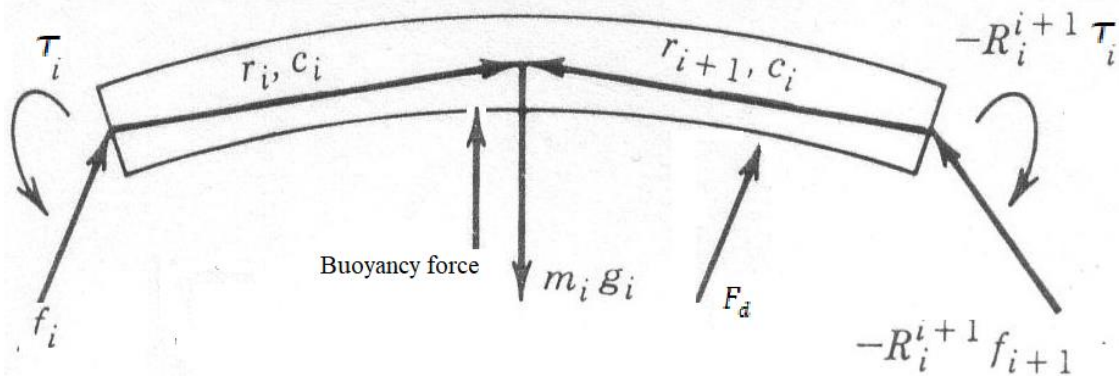


Figure 16. Free body diagram of forces and moments on link i .

where F_d is drag force, and f_i is the force applied by link $i - 1$ to link i . By law of action and reaction, link $i + 1$ applies a force of $-f_{i+1}^{i+1}$ to link i , expressed in frame $i + 1$. To express the same vector in frame i , we multiply it by the rotation matrix R_i^{i+1} . Similarly, it is repeated for action and reaction torque. $m_i g_i$ is the gravitational force, $a_{c,i}$ is the acceleration of the center of mass of link i . The force balance equation for link i is given by Equation (26).

$$f_i - R_i^{i+1} f_{i+1} + m_i g_i - F_b - F_d = m_i a_{c,i} \tag{26}$$

The moment balance equation for link i is given by Equation (27).

$$\tau_i - R_i^{i+1} \tau_{i+1} + f_i r_{i,c_i} - (R_i^{i+1} f_{i+1}) r_{i+1,c_i} = \alpha_i + \omega_i (I_i \omega_i) \tag{27}$$

When the robot moves in water, it also accelerates some water with it. The amount of fluid accelerated with the body is called added mass. The added-mass coefficients depend mainly on body geometry and can be regarded as the most important hydrodynamic characteristics [59]. The body of UMSWR is egg-shaped and fairly streamlined. For an egg-shaped body, it is analyzed as shown in Figure 17.

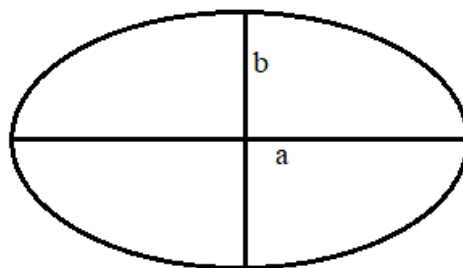


Figure 17. Added mass coefficient of egg-shaped body.

One convenient feature of added-mass coefficients is their symmetry, $m_{ij} = m_{ji}$. For symmetric bodies, the added mass tensor simplifies significantly. Among all three dimensions, ellipsoids are bodies for which comparable analytical results are available. Since there are three planes of symmetry, the nonzero added-mass coefficients are the six values of m_{ij} where $i = j$. The symmetry of the robot is such that the remaining added-mass coefficients are zero and there is no coupling between the three principal modes of motion of the body. The non-zero added mass co-efficient is given by Equation (28).

$$\left. \begin{aligned} m_{11} &= \pi\rho b^2 \\ m_{22} &= m_{33} = \pi\rho a^2 \\ m_{66} &= m_{55} = 1/8\pi\rho(a^2 - b^2)^2 \end{aligned} \right\} \tag{28}$$

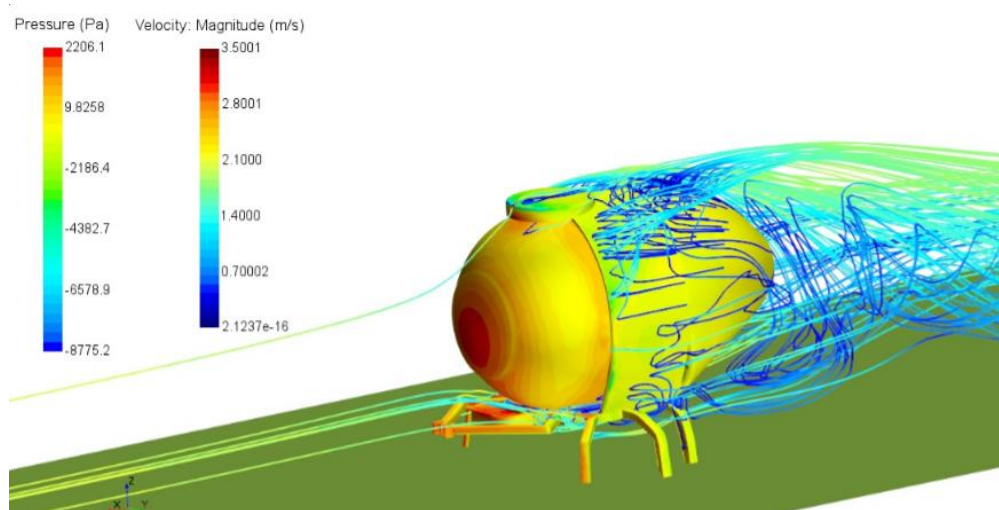
where m_{11} represent the longitudinal, $m_{22} = m_{33}$ lateral, and $m_{55} = m_{66}$ rotational added mass coefficients, respectively. It is assumed that the legs of the robot are nearly cylindrical. The added mass of the circular cylinder is equal to the displaced mass of fluid. The drag force can be decomposed into shear drag and pressure drag. For the underwater robot, shear drag is very small. Therefore, we neglect it, while considering only the pressure drag as many previous works have done [60].

$$F_d = \frac{1}{2}(\rho v^2 A C_d) \tag{29}$$

Drag term in Equation (29) is the function of joint angles, joint velocities, fluid velocity, and hydrodynamic coefficients determined by the geometries of links. For the underwater robot, the gravitational force is simply determined by its weight. Buoyancy force is calculated by Equation (30).

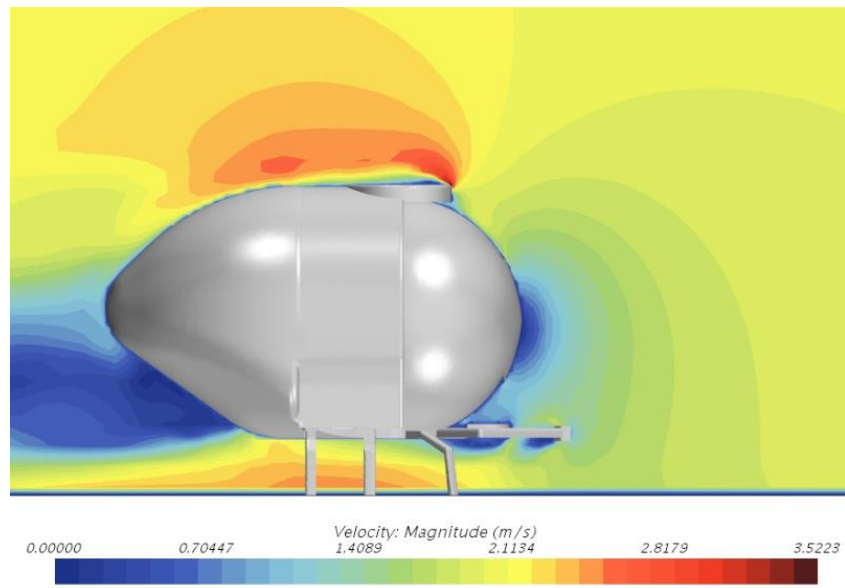
$$Buoyancy = \rho g \Delta \tag{30}$$

where Δ represents the volume of displaced mass of water, “g” is the gravitational acceleration (9.8 m/s²), and “ρ” is the density of the seawater. The current load depend on local climatic and geographic conditions. Current effects are added to the dynamics of the rigid body by considering the relative velocity in the body-fixed frame. The robot model is analyzed in Star CCM for drag force with a current of 2 m/sec in the opposite direction of motion. The results of the velocity and pressure distribution are shown in Figure 18 and drag force is shown in Figure 19.



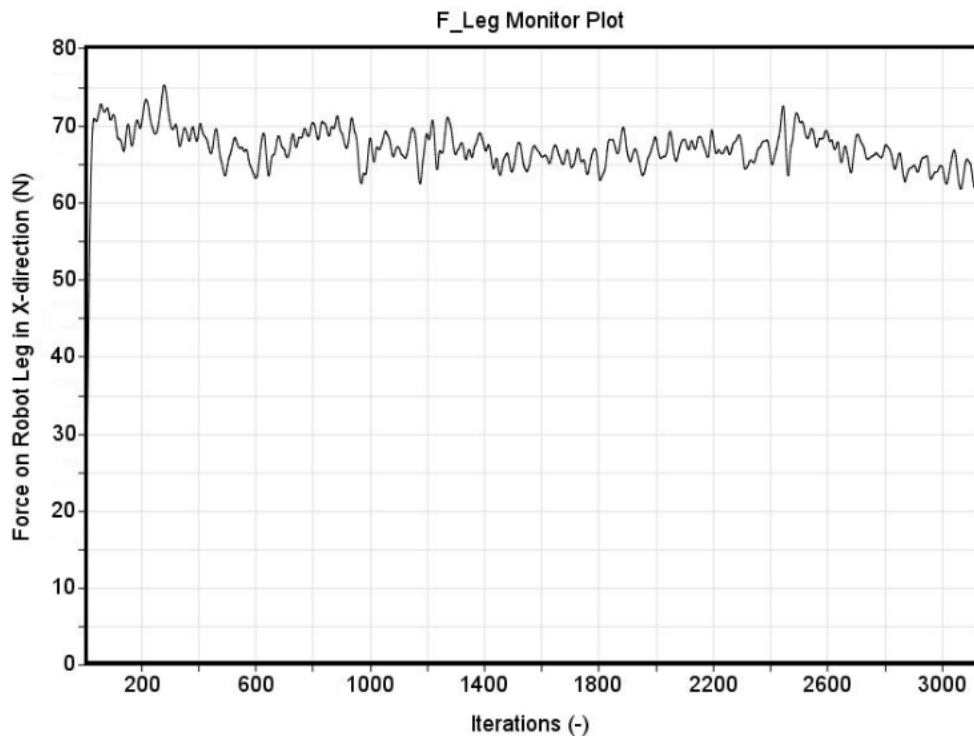
(a)

Figure 18. Cont.



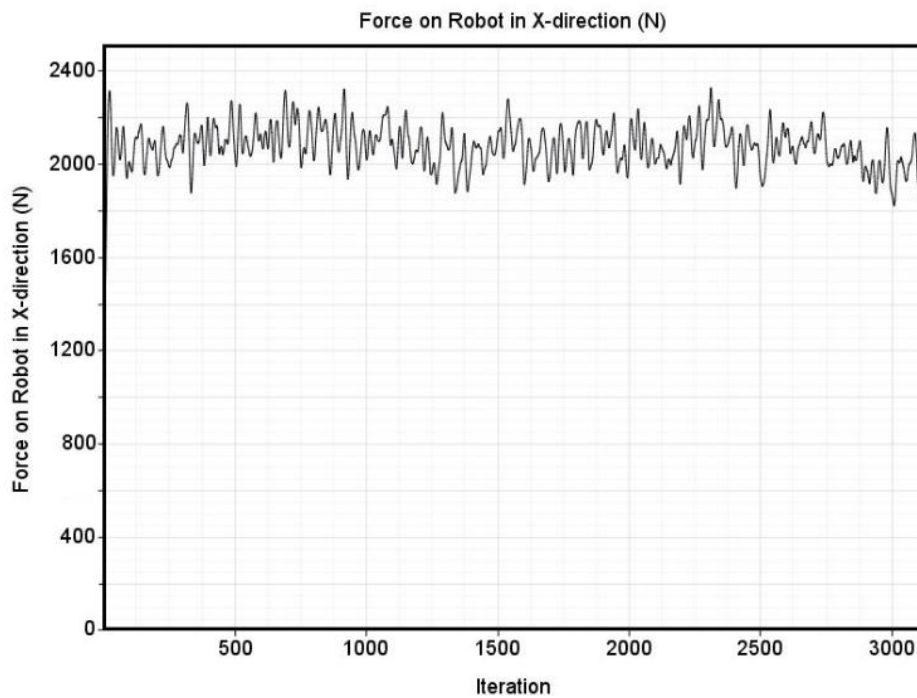
(b)

Figure 18. UMSWR analysis in shallow water. (a) Velocity and pressure distribution. (b) Velocity variation.



(a)

Figure 19. Cont.



(b)

Figure 19. Drag force evaluation on (a) leg. (b) Robot body.

A two-coordinate system is used for UMSWR, according to the Society of Naval Architects and Marine Engineers (SNAME) conventions (1950) [61]. These coordinates are the inertial frame of reference and body center called the body frame of reference, as shown in Figure 20.

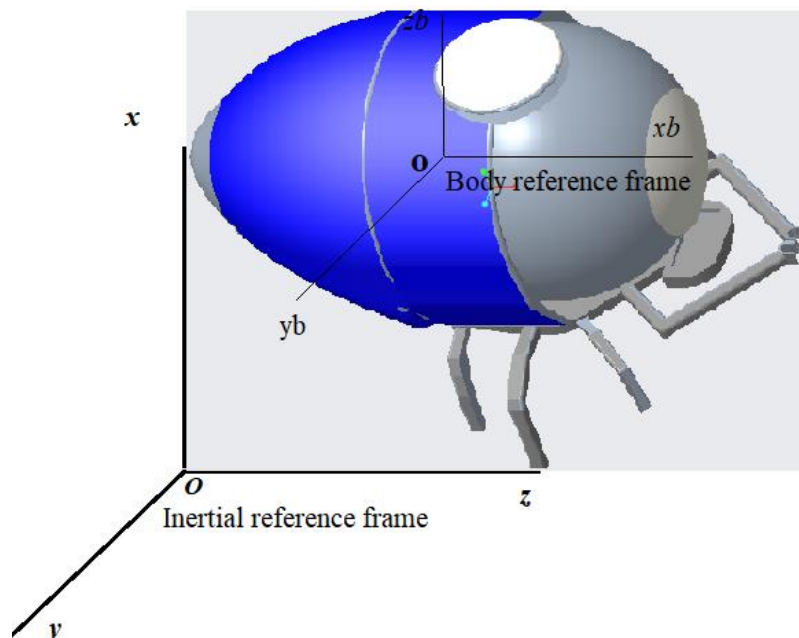


Figure 20. Representation of body and inertial reference frame.

3.4. Vertical Motion and Its Control Mechanism

Depth control of underwater platforms and the robot is a very important aspect as it needs to work at a required depth [12,62]. It makes sure that the robot goes to the expected depth to execute

the desired task and recovers to the surface when the task is finished. Vertical motion control shows nonlinear behavior and it is difficult for the robot to stop at a specific depth due to inertia. There is a strategy of combining hydrostatics, hydrodynamics, and kinematics analysis, so that the robot can stop at a specific depth with its velocity nearly becoming zero. The ballast tank system is used for controlling the diving and rising motion through water. It consists of main ballast tanks and trim tanks. Simple buoyance rules are exploited to undergo ascending and descending movements in water. The robot will be designed to dive or get to the surface rapidly under complete control. It will float on the surface and submerge at a desired rate of speed to its target depth. To do so quickly and efficiently, fore and aft balance and stability is maintained. The trim tank system is used to maintain fore and aft balance by controlling the amount and distribution of water in these tanks. When the robot is on the surface, the ballast tanks are filled with air and robot's overall density is less than that of the surrounding water. As it dives, the ballast tanks are flooded with water and air in the ballast tanks is vented until its overall density is greater than the surrounding water. Then the robot begins to dive. The ascending movement is similar to the descending movement. The dynamic equation of UMSWR when it descends in the heave direction can be simplified, as given by Equation (31).

$$F = m\ddot{x} = G - B - F_d \tag{31}$$

where "F" is the total net force on the robot, "m" is the total mass of the robot, "x" is the acceleration of the robot "G", weight of the robot, "B," is the buoyancy force on the robot, and "F_d" is the Drag force on the robot. The tether cable tension is neutralized by making it neutrally buoyant using a depressor that nullifies its effects. The depressor is attached with tether cable somewhere in water between the robot and power source. During diving or rising, the excess weight (G-B) is an important physical parameter. In the steady case of freely falling, when the robot reaches its terminal velocity, the excess weight is balanced by drag force [59]. Since we know that drag force depends on the projected area, the robot is adjusted such that it has optimum drag to balance the (B-G) term. It will ascend/descend in a safe and controlled manner throughout the depth of operations.

The estimated mass of the robot on the surface is approximately 1000 kg.

$$\text{Weight of robot} = W_1 = 1000 \times 9.8 = 9800 \text{ N}$$

$$\text{Volume of the robot} = V = 2.2\text{m}^3$$

Buoyancy force on the robot underwater has a fixed value since it is rigid and not effected by compression forces. The buoyancy force is given by Formula (32).

$$B = \rho g V \tag{32}$$

where ρ_w is the density of seawater (1025 kg/m³), g is the gravitational acceleration (9.8 m/s²), and V is the volume of the robot. Putting values in Equation (32).

$$B = 22,100 \text{ N}$$

Required ballast force for submergence is given by the equation below.

$$W_2 = B - W_1 = 22,100 - 9800 = 12,300 \text{ N}$$

$$\text{mass of ballast required} = m_1 = \frac{W_2}{g} = 1255 \text{ kg}$$

The volume of the ballast required for the submergence.

$$V_{ballast} = \frac{m_1}{\rho} = \frac{1255}{1.025} = 1.23\text{m}^3 \tag{33}$$

This implies that a ballast system of capacity 1.25 m^3 is required for diving motion underwater. Our target is to design a ballast system that can control the ascending and descending movements of the robot to target depth.

When the robot experiences movement through the water, a resistive force arise, acting on the robot in the direction of the relative fluid velocity, i.e., counteracting the robot transition direction. This force is called the drag force. This force depends on the robot projected area in the direction of motion, the drag coefficient, and the speed of the robot. The drag force is indicated by Equation (34).

$$F_d = \frac{1}{2} \rho v^2 C_d A \tag{34}$$

where v is the vertical speed of the robot, C_d is the drag coefficient, and A is the projected area of the robot. The drag force is also a variable that depends on projected area A and velocity $v = \dot{x}(t)$.

As water starts flooding in the ballast tanks, its weight starts increasing with a mass flow rate $\dot{m}(t)$. As the weight of the robot exceeds the buoyancy force, it starts going down. Compressed air that used for purging of the ballast tanks is assumed to have little impact comparatively. Therefore, we neglect its addition or subtraction. Drag force is changing with time, and, hence, the function of time.

$$W = f(t) = mg + \dot{m}1g \tag{35}$$

$$F_d = g(t) = \frac{1}{2} \rho v^2 C_d A = \frac{1}{2} \rho (\dot{x}(t))^2 C_d A \tag{36}$$

where $\dot{m}1$ is the rate of mass flow to the ballast tank. We are interested merely in velocity $\dot{x}(t)$ and position $x(t)$ of the robot and the time t it take to reach the target depth. Putting values of drag force, the weight of the robot, and the buoyancy force in Equation (31), we get the following.

$$m\ddot{x} = (mg + \dot{m}1g) - \rho gV - \left(\frac{1}{2} \rho (\dot{x})^2 C_d A\right) \tag{37}$$

$$\ddot{x}(t) = \dot{v}(t) = \frac{(mg + \dot{m}1g) - \rho gV - \left(\frac{1}{2} \rho (\dot{x})^2 C_d A\right)}{m} \tag{38}$$

This is a second order differential equation describing the motion of the UMSWR as a function of time while taking drag force into account. Integrating Equation (38), the results of the vertical velocity of the robot are shown below.

$$\dot{x}(t) = v(t) = \int \frac{(mg + \dot{m}1g) - \rho gV - \left(\frac{1}{2} \rho (\dot{x})^2 C_d A\right)}{m} dt \tag{39}$$

Integrating Equation (39) yields distance covered after time t .

$$x(t) = \iint \frac{(mg + \dot{m}1g) - \rho gV - \left(\frac{1}{2} \rho (\dot{x})^2 C_d A\right)}{m} dt dt \tag{40}$$

The amount of water that leaves or enters the ballast is defined as $\dot{m} \cdot \Delta t = m_{step}$ and can be assumed that, for every time step Δt , there exists three mutually exclusive actions.

- (a) Flooding mass = $\dot{m}1 \cdot \Delta t \cdot input$
- (b) Discharging mass = $-\dot{m}1 \cdot \Delta t \cdot input$
- (c) Do nothing = $\dot{m}1 \cdot \Delta t = 0$

Where input is a variable number such that $-1 \leq input \leq +1$ that represents the opening of the valve. The mass of the water inside the ballast tanks at time t is a sum of the number of operations, which are added up over the series of n time-steps.

$$m(t, input) = \sum_{t=i=0}^n [\dot{m} \cdot \Delta t \cdot input_{t=n}] \tag{41}$$

$$\text{With } \begin{cases} input < 0 : \dot{m} = discharge \\ input > 0 : \dot{m} = flooding \\ input = 0 : \dot{m} = 0 \end{cases} \tag{42}$$

The robot will maintain an acceptable stability and trim during the ascent and descent, while submerged and on the surface. Acceptable stability and trim shall be maintained during transit from a submerged to a surfaced condition, and vice versa. The robot will be deployed on the sea surface from a ship or any other floating platform on a desired location for an intended operation. It is positively buoyant when at surface with aft and stern are at the same level. The robot is capable of remaining on the surface with the top hatch open during all anticipated design environmental and operating conditions without down flooding. The robot is equipped with two lifting points to which attachments may be secured to raise the robot to the surface in emergency conditions without assistance from the pilot. The underwater stability is to be maintained positive in all situations. The height GB of the center of buoyancy above the center of gravity is to be adjusted such that it is not less than 50 mm in normal loading and ballasting [40].

3.5. Path Planning for Optimized Drag and Posture Adjustment Technique

We take Drag-optimization and posture adjustment technologies fifth in importance in UMSWR. Legged robots are preferred over other types of mobile robots because of their ability to navigate on uneven and rough terrain but this has not been yet fully exploited. It is due to a lack of an adequate motion planner capable of computing unique sequences of footsteps and postural adjustments to adapt to the local terrain [63]. For efficient underwater walking, the joint path of legs are planned so that the hydrodynamic forces are optimized. For optimized path planning, the joint constraints e.g., joints angles (θ), angular velocities ($\dot{\theta}$), accelerations ($\ddot{\theta}$), and torques (τ), are considered. Optimal gait path parameters minimize the objective function given by Equation (43).

$$g = \int_0^T \|D(C_D, \theta, \dot{\theta})\| dt \tag{43}$$

where g represents the gait parameter, D represents the drag force, C_D is the drag coefficient, θ is the joint variable, and $\dot{\theta}$ is the joint velocity. Equation (43) is valid when only subjected to inequality in Equation (44), which defines the joint constraints' bounds.

$$\begin{aligned} \theta_{i,min} &\leq \theta_i \leq \theta_{i,max} \\ \dot{\theta}_{i,min} &\leq \dot{\theta}_i \leq \dot{\theta}_{i,max} \\ \ddot{\theta}_{i,min} &\leq \ddot{\theta}_i \leq \ddot{\theta}_{i,max} \\ \tau_{i,min} &\leq \tau_i \leq \tau_{i,max} \end{aligned} \tag{44}$$

Note : ($i = 1 - n$. for leg $n = 4$ & for arm $n = 6$)

Joint constraints' bounds can be found by vector transformation (45).

$$X \equiv D\theta + X_0 \tag{45}$$

where

$$\theta = [\theta_1 \dots \theta_n]^T \tag{46}$$

$$D \equiv \text{diag}\left[\frac{2}{\theta_{1,max} - \theta_{1,min}} \dots \dots \frac{2}{\theta_{n,max} - \theta_{n,min}}\right] \tag{47}$$

$$X_0 \equiv \left[-\frac{\theta_{1,max} + \theta_{1,min}}{\theta_{1,max} - \theta_{1,min}} \dots \dots -\frac{\theta_{n,max} + \theta_{n,min}}{\theta_{n,max} - \theta_{n,min}}\right]^T \tag{48}$$

In gait planning, legs redundancy can be resolved in the sense of drag-optimization. It is very important to control the position and posture of the robot, while walking and performing the task. A good performance for a walking robot can be simply defined as to arrive to a goal point without falling down, by observing a suitable ground reaction force to keep the dynamic balance.

The main concept of UMSWR states that it should have working ability in both deep water and a high tidal current environment. In order to prevent overturn against water currents, for the posture compensation, the robot will adjust the body posture according to the velocity and direction of the water current. Calculating drag and lift forces act on the robot body and legs for each posture by the CFD analysis tool (Star CCM+). If we have lift and drag forces values, the stability criteria of UMSWR can be driven from Figure 21 by Equation (49).

$$(mg + B + F_f) \leq F_e F_d \tag{49}$$

where m is the mass of the robot, B is the buoyancy force, F_e is the external force, F_f is the friction force ($F_f = \mu F_l$), μ is the co-efficient of friction force, F_l is the lift force, and F_d is the drag force on the robot. Since drag and lift forces are functions of water current velocity and robot posture, the inequality functions (49) can be satisfied by adjusting the posture of the robot. Consequently, we can utilize the water currents to improve the stability margin of UMSWR. For this function, UMSWR has a velocity log, a force/torque sensor, an attitude sensor, and a ground reaction force sensor.

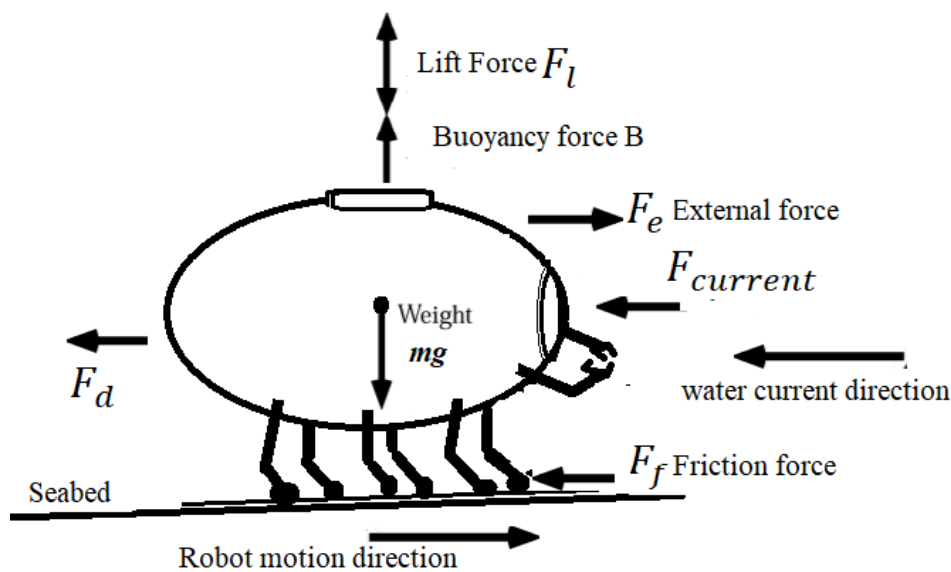


Figure 21. UMSWR seabed operation concept for posture adjustment.

Legged robots have the ability to change 3-DoF position and 3-DoF posture of the body and can control full 6-DoF without changing the contact condition between legs and ground within its range. Utilizing a balancing control approach for regulating the center of the mass position and body orientation. It allows the robot to adapt compliantly to unknown external perturbation forces. The system can be analyzed as a series of contact forces applied at the contact points, which generate a net wrench on the robot called the ground reaction force. A desired wrench is applied at the COM of the robot, generated through forces at the contact points. The force to be generated is called the ground applied force. The approach of creating a balancing controller to distribute a desired ground

applied force to all the contact points, such that they guarantee a net desired wrench on the robot. For this purpose, the sensors will be installed such as the force/torque sensor, the attitude sensor, and the ground reaction force sensor.

Path planning of a hexapod robot walking on the seabed is very complex for accomplishing the given task. The main body of the UMSWR and swing leg have an uninterrupted and continuous motion for the given initial position and orientation. Hence, it is assumed that the motions are regulated by a step function that approximates the Heaviside step function with a cubic polynomial [64]. Effective gait planning and an efficient algorithm is required to move the robot's legs in a sequential manner along a straight path on various terrains. For calculation, at the start of motion, the initial rate of change of displacement of the main body is considered to be d_0 . The maximum rate of change of linear displacement is d_1 . The total time of motion of the robot is equivalent to the time taken to complete n duty cycles, which is given by Equation (50).

$$s|_n = t_3 \tag{50}$$

where s stands for swing. t_3 is calculated by Equation (51).

$$t_3 = t_0 + 2\Delta t + (1/d_1) \left[s_T - \left(d_0 + \frac{d}{2} \right) \left(\frac{1}{\Delta_{a'}} \right) - (d_1 - d/2) \cdot (1/\Delta_{d'}) \right] \tag{51}$$

$$d = d_0 - d_1 \tag{52}$$

Assuming that

$$\Delta t = t_1 - t_0 = t_3 - t_2 \tag{53}$$

$$s = n \cdot (k d_b) \tag{54}$$

where s is the total distance covered, k is the number of divisions of gait cycle. In the present case: $k = 6$, d_b is the displacement of the main body per division in a gait cycle, $\Delta_{a'}$ and $\Delta_{d'}$ are the first derivatives of acceleration and deceleration with respect to time, respectively. Δt is the duration of acceleration and deceleration of the main body, t_0 is the start time, t_1 is the end time of acceleration, and t_2 is the start time of retardation.

For UMSWR motion:

$$d_0 = \dot{X} \Big|_{t=t_0} \tag{55}$$

$$d_1 = \dot{X} \Big|_{t=t_1} \tag{56}$$

Displacement, velocity, acceleration, and center of gravity are evaluated for the main body motion, the swing leg trajectory planning of the feet-tip, and specified gait planning on various terrains. These outputs are, subsequently, transformed from an inertial reference frame to the body-centered reference frame, such that the velocity and acceleration vectors of the link ij with respect to the body-centered reference frame are represented by the equations below.

$$v_{ij} = \left((\dot{r}_{ij})^T, (\dot{\omega}_{ij})^T \right)^T \in R^{144} \tag{57}$$

$$\dot{v}_{ij} = \left((\ddot{v}_{ij})^T, (\ddot{\omega}_{ij})^T \right)^T \in R^{144} \tag{58}$$

where $i = 1-6$ and $j = 1-4$ and r_{ij} is the displacement vector of the point P_{ij} on link i and Joint j with respect to the body-centered reference frame O_b . These values of the velocities and accelerations are used to carry out dynamic analysis of the system for evaluating feet forces and joint torques.

In addition, there are various other technologies for some specialized purpose. The body frame of UMSWR will consist of carbon fiber reinforced plastic (CFRP) because of its light weight, water

resistant, and strength. Inside the sphere are two smaller HD cameras that, together, capture 3-D video of the pilot and one HD camera capturing outside the video. All the technologies installed in other underwater robots that are appropriate may be utilized and shared with UMSWR. A highly illuminating LED system installed in the frontal section that enable the operator to look around in the underwater environment.

4. Conclusions

A novel concept design of an underwater walking robot is presented. The robot is different from both conventional screw-propelled robot and underwater walking, remotely operated robots. The proposed robot will be operated by a pilot sitting in the spherical pressure hull, which is an integrated part of the robot. The main concept is development of a robot that can walk on seabed calmly. The robot will be using six legs for walking and two arms for a manipulation function. The manipulator arms can also be used for walking and enhanced stability. Each leg having four joints instead of the required three joints, enhances its stability and flexibility in posture adjustment. All the legs and arms with 36 joints are controlled by BLDC motors. The robot is powered by an external power source through a tether cable. The proposed robot is a combination of submersible, AUV, ROV, and terrestrial walking robot. All the fundamental technologies identified for the development of the robot and their approaching methods to develop these technologies are presented. These include manned pressure vessel technology, underwater joints and walking mechanism, modeling and analysis of hydrodynamic forces, vertical motion and a buoyancy control mechanism, path planning for optimized drag, and posture adjustment technologies. It will provide a safe operation space for humans in deep-sea exploration and operation. Its ability to walk and work underwater on the seabed will make it a useful working platform for a variety of underwater applications.

Author Contributions: Conceptualization, A.K., W.L., and W.G.; Data curation, A.K. and W.G.; Formal analysis, A.K. and W.G.; Funding acquisition, W.L.; Investigation, A.K.; Methodology, A.K.; Project administration, W.L.; Resources, W.L.; Software, M.I.; Supervision, W.L. and W.G.; Validation, M.I.; Visualization, H.M.W.; Writing—review & editing A.A.Z.

Funding: This research was funded by National Natural Science Foundation of China ' Sealing Performance and Multi-Objective Structural Optimization of Deep-Sea Connector Under High Gradient Temperature Fluctuation ' grant number (5177090429).

Conflicts of Interest: The authors declare no conflict of interest.

References

1. Ji, W.S.; Cho, B.K. Development of a walking algorithm on the uneven terrain for a hexapod robot Little Crabster200. *Adv. Mech. Eng.* **2018**, *10*, 1–12. [CrossRef]
2. NOAA. How Much of the Ocean Have We Explored? Available online: www.oceanservice.noaa.gov/facts/exploration (accessed on 10 July 2019).
3. Shim, H.; Yoo, S.; Kang, H.; Jun, B. Development of arm and leg for seabed walking robot CRABSTER200. *Ocean Eng.* **2016**, *116*, 55–67. [CrossRef]
4. Larkum; Broome. Advanced controller for an underwater manipulator. In Proceedings of the IEEE International Conference on Control and Applications, Glasgow, UK, 24–26 August 1994; pp. 1081–1086.
5. Antsaklis, P.J.; Passino, K.M. *An Introduction to Intelligent and Autonomous Control*; Antsaklis, P.J., Passino, K.M., Eds.; Kluwer Academic Publishers: Norwell, MA, USA, 1993; pp. 1–26.
6. Dong, M.; Chou, W. Vertical Motion Control of Underwater Robot Based on Hydrodynamics and Kinematics Analysis. In Proceedings of the 2017 IEEE International Conference on Robotics and Biomimetics (ROBIO), Macau, China, 5–8 December 2017; pp. 2–7.
7. Molnar, L.; Omerdic, E.; Toal, D. Design of an advanced AUV for deployment close to the seabed and other hazards. In Proceedings of the Europe Oceans 2005, Brest, France, 20–23 June 2005; Volume 2, pp. 975–980.
8. Kang, H.; Shim, H.; Jun, B.H.; Lee, P.M. Development of leg with arm for the multi-legged seabed robot "CR200". In Proceedings of the Ocean 2012 MTS/IEEE Harnessing Power Ocean, Hampton Roads, VA, USA, 14–19 October 2012; pp. 1–4.

9. Wronka, C.M.; Dunnigan, M.W. Derivation and analysis of a dynamic model of a robotic manipulator on a moving base. *Robot. Auton. Syst.* **2011**, *59*, 758–769. [[CrossRef](#)]
10. Ayers, J.; Witting, J. Biomimetic approaches to the control of underwater walking machines. *Philos. Trans. R. Soc. A Math. Phys. Eng. Sci.* **2007**, *365*, 273–295. [[CrossRef](#)] [[PubMed](#)]
11. Othman, M.N. Problem Identification for Underwater Remotely Operated Vehicle (ROV): A Case Study. *Procedia Eng.* **2012**, *41*, 554–560.
12. Tang, Z.; Yan, P.; Jun, L. A novel ROV depth control based on LSM fitting predictor and fuzzy compensation. In Proceedings of the 2010 3rd International Conference on Advanced Computer Theory and Engineering (ICACTE), Chengdu, China, 20–22 August 2010; Volume 2, pp. 2–614.
13. Purcell, M.; Gallo, D.; Packard, G.; Dennett, M.; Rothenbeck, M.; Sherrell, A.; Pascaud, S. Use of REMUS 6000 AUVs in the search for the Air France Flight 447. In Proceedings of the OCEANS'11 MTS/IEEE KONA, Waikoloa, HI, USA, 19–22 September 2011; pp. 1–7.
14. Kang, H.; Shim, H.; Jun, B.; Lee, P. Design of the Underwater Link-Joint System for the Multi-Legged Underwater Robot “CR200”. In Proceedings of the 2012 Ocean-Yeosu, Yeosu, Korea, 21–24 May 2012; pp. 1–6.
15. Kim, B.; Shim, H.; Yoo, S.Y.; Jun, B.H.; Park, S.W.; Lee, P.M. Operating software for a multi-legged subsea robot CR200. In Proceedings of the OCEANS 2013 MTS/IEEE Bergen: The Challenges of the Northern Dimension, Bergen, Norway, 10–14 June 2013; pp. 1–5.
16. Wang, G.; Chen, X. Experimental and numerical study on hydrodynamics of swimming paddle for a shoal crab robot. In Proceedings of the OCEANS 2017-Aberdeen, Aberdeen, UK, 19–22 June 2017; pp. 1–10.
17. Tanaka, T.; Sakai, H.; Akizono, J. Design concept of a prototype amphibious walking robot for automated shore line survey work. In Proceedings of the Oceans '04 MTS/IEEE Techno-Ocean '04 (IEEE Cat. No. 04CH37600), Kobe, Japan, 9–12 November 2004; Volume 2, pp. 834–839.
18. Cubero, S.N. Design concepts for a hybrid swimming and walking vehicle. *Procedia Eng.* **2012**, *41*, 1211–1220. [[CrossRef](#)]
19. Yoo, S.; Jun, B.; Shim, H.; Lee, P. Design and analysis of carbon fiber reinforced plastic body frame for multi-legged subsea walking robot, Crabster. *Ocean Eng.* **2015**, *102*, 78–86. [[CrossRef](#)]
20. Jun, B.H.; Shim, H.; Kim, B.; Park, J.Y.; Baek, H.; Yoo, S.; Lee, P.M. Development of seabed walking robot CR200. In Proceedings of the 2013 MTS/IEEE OCEANS, Bergen, Norway, 10–14 June 2013; pp. 1–5.
21. Jun, B.H.; Shim, H.; Kim, B.; Park, J.Y.; Baek, H.; Lee, P.M.; Kim, W.J.; Park, Y.S. Preliminary design of the multi-legged underwater walking robot CR200. In Proceedings of the 2012 Oceans-Yeosu, Yeosu, Korea, 21–24 May 2012; pp. 1–4.
22. ROBOT CRAB CLEANS WASTE FROM OCEAN FLOOR The Crab Robot SILVER 2. Available online: www.santannapisa.it/e (accessed on 2 July 2019).
23. Georgiades, C. *Simulation and Control of an Underwater Hexapod Robot*; McGill University: Montreal, QC, Canada, 2005.
24. Ariel. The Mine Hunter Robot. Available online: <https://www.irobot.it/inews/ariel.php> (accessed on 2 September 2019).
25. Kim, J.Y.; Jun, B.H. Design of six-legged walking robot, Little Crabster for underwater walking. *Adv. Robot.* **2013**, *28*, 77–89. [[CrossRef](#)]
26. Du, W.; Mo, R.; Li, S. Key characteristics extraction method in product concept design. In Proceedings of the 2011 International Conference on Computer Science and Network Technology, Harbin, China, 24–26 December 2011; pp. 2169–2173.
27. Cockton, G. Conceptual Design. In *Engineering for Human-Computer Interaction*; Larson, J., Unger, C., Eds.; Chapman and Hall: Yellowstone Park, WY, USA, 1996.
28. Watson, D.G.M. *Practical Ship Design*, 2nd ed.; British Library of Congress: Tokyo, Japan, 1998; Volume 1.
29. Physiology, A.; Sleininis, S.; Silvey, G.E. Locomotion in a forward walking crab. *J. Com. Phys. A Neuroethol. Sens. Neural Behav. Phys.* **1980**, *136*, 301–312.
30. Klaassen, B.; Linnemann, R.; Spenneberg, D.; Kirchner, F. Biomimetic walking robot SCORPION: Control and modeling. *Robot. Auton. Syst.* **2002**, *41*, 69–76. [[CrossRef](#)]
31. Wimböck, T.; Görner, M.; Hirzinger, G. The DLR Crawler: Evaluation of gaits and control of an actively compliant six-legged walking robot. *Ind. Robot Int. J. Robot Res. Appl.* **2009**, *36*, 344–351.
32. Lewinger, W.A.; Quinn, R.D. Neurobiologically-based control system for an adaptively walking hexapod. *Ind. Robot Int. J. Robot Res. Appl.* **2011**, *38*, 258–263. [[CrossRef](#)]

33. Alex, A.; Giuffré, G.P.; Forès, P.; Roca, J.; Parareda, C.; Roca, A. Pressure Hull Design and Construction of the Manned. *Instrum. Viewp.* **2009**, *3*, 35–36.
34. Yuh, J. Design and Control of Autonomous Underwater Robots: A Survey. *Auton. Robots* **2000**, *8*, 7–24. [[CrossRef](#)]
35. Binbin, P.; Weicheng, C. On an appropriate design and test standard for spherical pressure hull in a deep manned submersible. In Proceedings of the 2011 IEEE Symposium on Underwater Technology and Workshop on Scientific Use of Submarine Cables and Related Technologies, Tokyo, Japan, 5–8 April 2011; pp. 1–7.
36. Pan, B.B.; Cui, W.C. A comparison of different rules for the spherical pressure hull of deep manned submersibles. *Mar. Struct. Rev.* **2011**, *15*, 276–285.
37. Alcocer, A.; Forès, P.; Piero Giuffré, G.; Parareda, C.; Roca, A.; Roca, J. Pressure hull design and construction of the manned submersible Ictineu 3. *Instrum. Viewp.* **2009**, *8*, m3.
38. Pan, B.; Cui, W. An overview of buckling and ultimate strength of spherical pressure hull under external pressure. *Mar. Struct.* **2010**, *23*, 227–240. [[CrossRef](#)]
39. Camero, J. Deep Sea Challenger. Available online: <http://www.deepseachallenge.com/the-sub/> (accessed on 2 May 2019).
40. China Classification Society Rules for Certification of Diving System and Submersible 2018. Available online: <https://www.ccs.org.cn/ccswzen/font/fontAction!article.do?articleId=4028e3d6660ffd5f01692c9355f60313> (accessed on 2 July 2019).
41. Oryshchenko, A.S.; Gorynin, I.V.; Leonov, V.P.; Kudryavtsev, A.S.; Mikhailov, V.I.; Chudakov, E.V. Marine titanium alloys: Present and future. *Inorg. Mater. Appl. Res.* **2015**, *6*, 571–579. [[CrossRef](#)]
42. Matthew, D.J. (Ed.) *Titanium: A Technical Guide*, 2nd ed.; ASM Internationa: Almere, The Netherlands, 2000.
43. Chu, P.K.; Lu, X.P. *Low Temperature Plasma Technology: Methods and Applications*; CRC Press: Boca Raton, FL, USA, 2013.
44. Zhang, J.; Wang, M.; Wang, W.; Tang, W.; Zhu, Y. Investigation on egg-shaped pressure hulls. *Mar. Struct.* **2017**, *52*, 50–66. [[CrossRef](#)]
45. Zhu, Y.; Dai, Y.; Ma, Q.; Tang, W. Buckling of externally pressurized cylindrical shell: A comparison of theoretical and experimental data. *Thin Walled Struct.* **2018**, *129*, 309–316. [[CrossRef](#)]
46. Zhang, J.; Zhu, B.; Wang, F.; Tang, W.; Wang, W.; Zhang, M. Buckling of prolate egg-shaped domes under hydrostatic external pressure. *Thin Walled Struct.* **2017**, *119*, 296–303. [[CrossRef](#)]
47. Wagner, H.N.R.; Hühne, C.; Niemann, S. Robust knockdown factors for the design of spherical shells under external pressure: Development and validation. *Int. J. Mech. Sci.* **2018**, *141*, 58–77. [[CrossRef](#)]
48. Zhang, M.; Tang, W.; Wang, F.; Zhang, J.; Cui, W.; Chen, Y. Buckling of bi-segment spherical shells under hydrostatic external pressure. *Thin Walled Struct.* **2017**, *120*, 1–8. [[CrossRef](#)]
49. Ventsel, E.; Krauthammer, T. *Thin Plates and Shells*, 1st ed.; Taylor & Francis: Boca Raton, FL, USA, 2001.
50. ASME. *ASME PHVO-1 2007*; ASME: New York, NY, USA, 2007; Volume 1.
51. Cui, W. Development of the Jiaolong deep manned submersible. *Mar. Technol. Soc. J.* **2013**, *47*, 37–54. [[CrossRef](#)]
52. Chen, J.; Liu, Y.; Zhao, J.; Zhang, H.; Jin, H. Biomimetic Design and Optimal Swing of a Hexapod Robot Leg. *J. Bionic Eng.* **2014**, *11*, 26–35. [[CrossRef](#)]
53. Gang, W.; Xi, C. Mechatronics Subsea crab bounding gait of leg-paddle hybrid driven shoal crablike robot. *Mechatronics* **2017**, *48*, 1–11.
54. Abolvafaie, M.; Koofgar, H.R.; Malekzadeh, M. Classification of Hydrodynamic Coefficients of Autonomous Underwater Vehicles based on sensitivity analysis in Standard Maneuvers. *J. Mar. Sci. Technol.* **2018**, *26*, 1–10.
55. Li, Z.; Tao, J.; Sun, H.; Luo, Y.; Ding, L. Hydrodynamic calculation and analysis of a complex-shaped underwater robot based on computational fluid dynamics and prototype test. *Adv. Mech. Eng.* **2017**, *9*, 1–10. [[CrossRef](#)]
56. Yue, C.; Guo, S.; Shi, L.; Paper, R.; Yue, C.; Guo, S.; Shi, L. Hydrodynamic analysis of the Spherical Underwater Robot SUR-II. *Int. J. Adv. Robot. Syst.* **2013**, *10*, 1–12. [[CrossRef](#)]
57. Antonelli, G.; Fossen, T.I.; Yoerger, D.R. Underwater Robotics. In *Springer Handbook of Robotics*; Springer: Berlin/Heidelberg, Germany, 2008.
58. Fossen, T.I. *Marine Craft Hydrodynamics*, 1st ed.; John Wiley & Sons: Hoboken, NJ, USA, 2011.
59. Newman, J.N. *Marine Hdrodynamics*, 40th ed.; Library of Congress: Washington, DC, USA; The MIT Press: Cambridge, MA, USA, 2017.

60. Jun, B.H.; Shim, H.; Park, J.Y.; Kim, B.; Lee, P.M. A new concept and technologies of multi-legged underwater robot for high tidal current environment. In Proceedings of the 2011 IEEE Symposium on Underwater Technology and Workshop on Scientific Use of Submarine Cables and Related Technologies, Tokyo, Japan, 5–8 April 2011; pp. 3–7.
61. SNAME. Society of Naval Architects and Marine Engineers. Available online: <https://www.sname.org/> (accessed on 15 July 2019).
62. Chen, T.; Zhang, W.; Zhou, J.; Yu, H.; Liu, X.; Hao, Y. Depth control of AUV using active disturbance rejection controller. In Proceedings of the 33rd Chinese Control Conference, Nanjing, China, 28–30 July 2014.
63. Bálint, K.; István, H.; Béla, L. Motion Planning for Legged Robots. *SIAM J. Comput.* **2000**, *30*, 218–246.
64. Mahapatra, A.; Roy, S.S.; Pratihari, D.K. Study on feet forces' distributions, energy consumption and dynamic stability measure of hexapod robot during crab walking. *Appl. Math. Model.* **2019**, *65*, 717–744. [[CrossRef](#)]



© 2019 by the authors. Licensee MDPI, Basel, Switzerland. This article is an open access article distributed under the terms and conditions of the Creative Commons Attribution (CC BY) license (<http://creativecommons.org/licenses/by/4.0/>).